Electronic Supplementary Information

Selective Sensing of Picric Acid using a Zn(II)-metallacycle: Experimental and Theoretical Validation of Sensing Mechanism and Quantitative Analysis of Sensitivity in Contact Mode Detectionusing Zn(II) metallacycle

Vishakha Jaswal[a], Sanya Pachisia[b,c], Jagrity Chaudhary[d], Krishnan Rangan[e], and Madhushree Sarkar*[a]

[a]Department of Chemistry, Birla Institute of Technology and Science, Pilani, Pilani Campus, Rajasthan 333031 India.

E-mail: msarkar@pilani.bits-pilani.ac.in

[b] Department of Chemistry, University of Delhi, India.

[c] Department of Chemistry, University of California, Irvine, California, USA.

[d] Department of Chemistry, Purdue University, West Lafayette, Indiana, USA

[e] Department of Chemistry, BITS Pilani, Hyderabad Campus, Jawahar Nagar Shameerpet Mandal, Ranga Reddy District, Hyderabad 500078, India

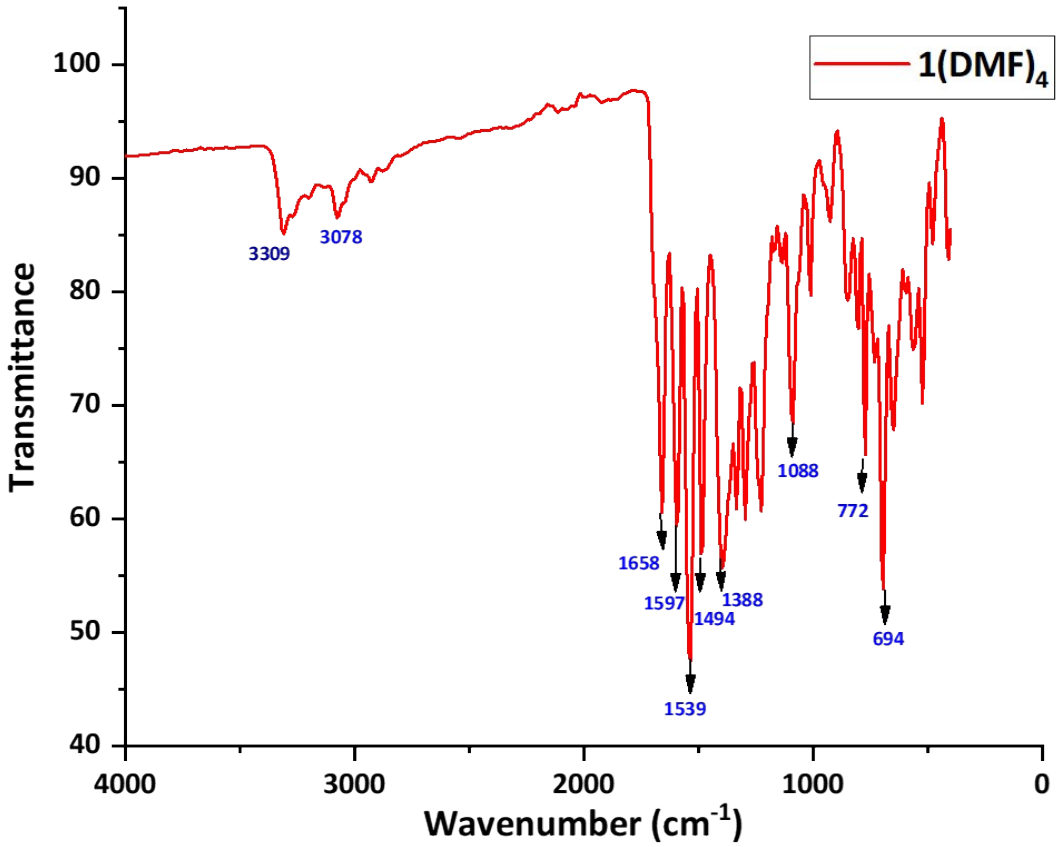

Figure S1. IR Spectrum of **1(DMF)$_4$**.

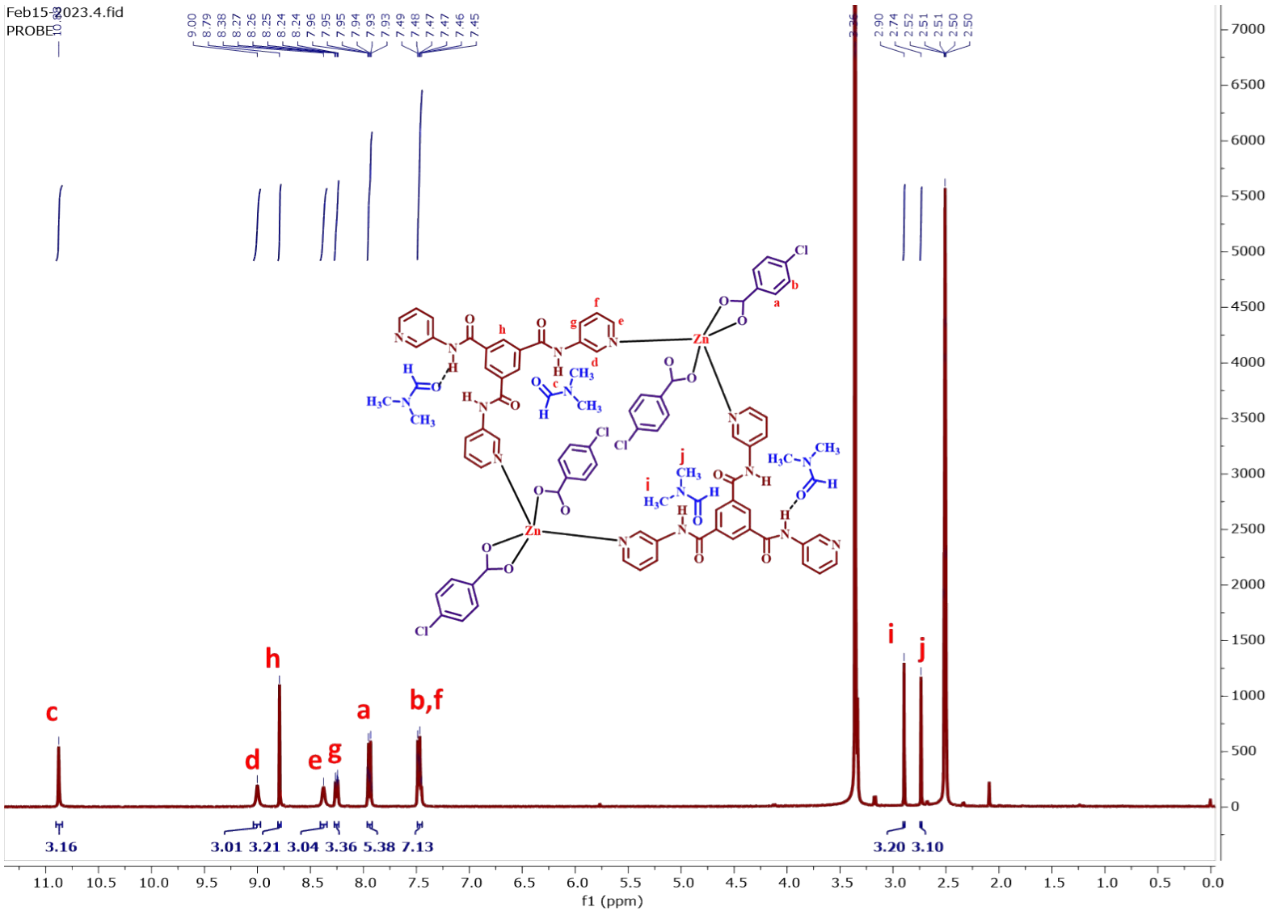

Figure S2. ^{1}H-NMR (DMSO-d_6) spectrum of **1(DMF)$_4$**.

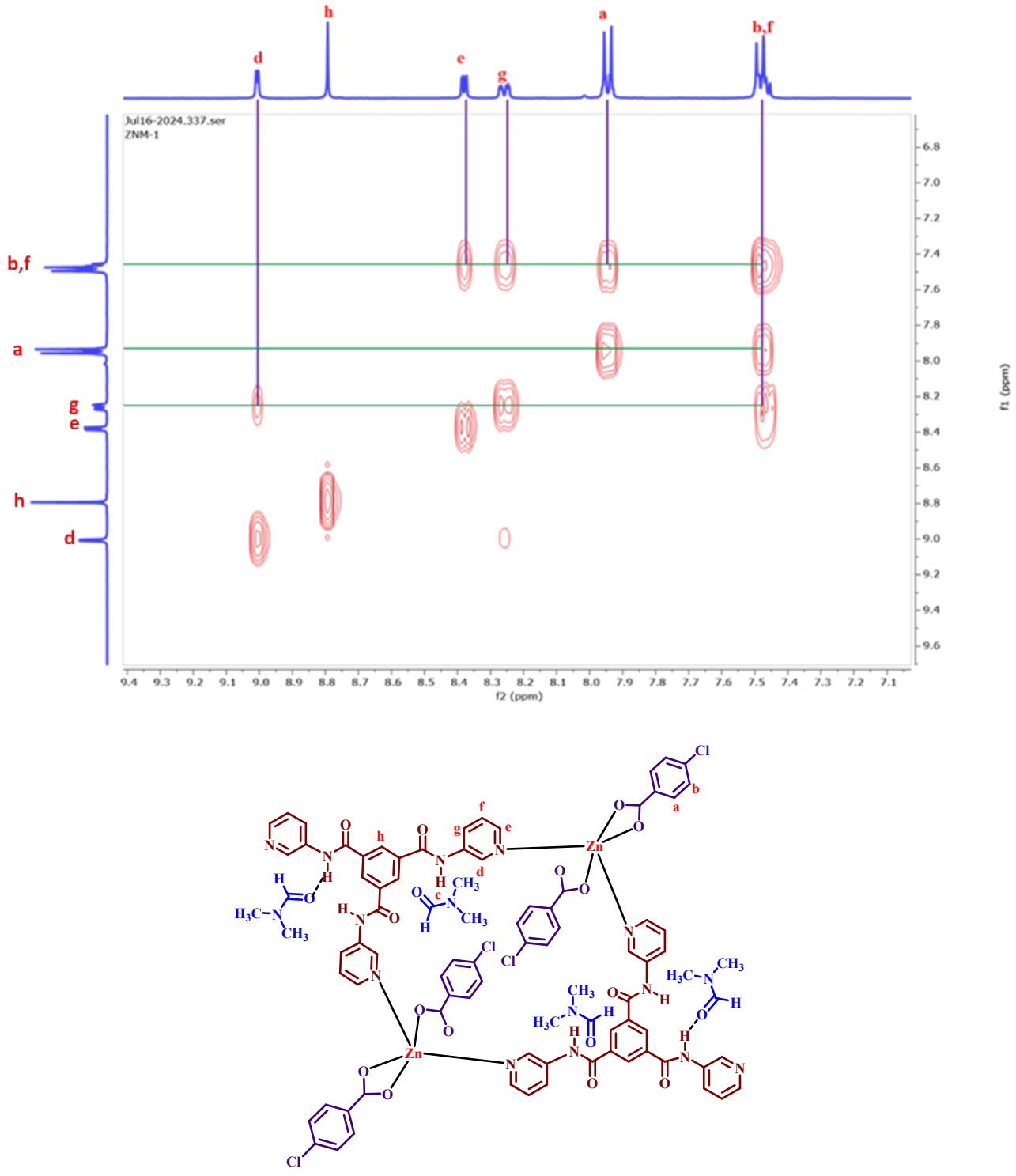

Figure S3. COSY-NMR (DMSO-d_6) spectrum of **1(DMF)$_4$**.

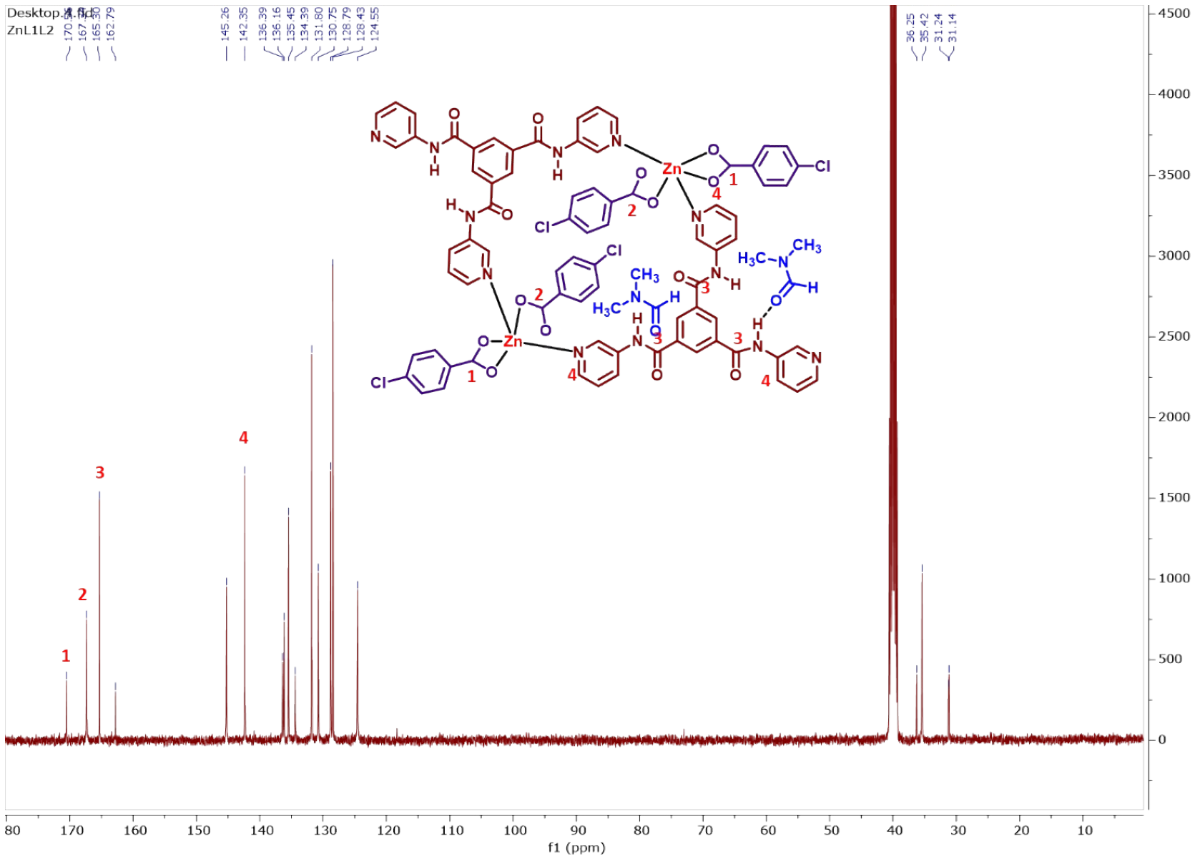

Figure S4. ^{13}C-NMR (DMSO-d_6) spectrum of **1(DMF)$_4$**.

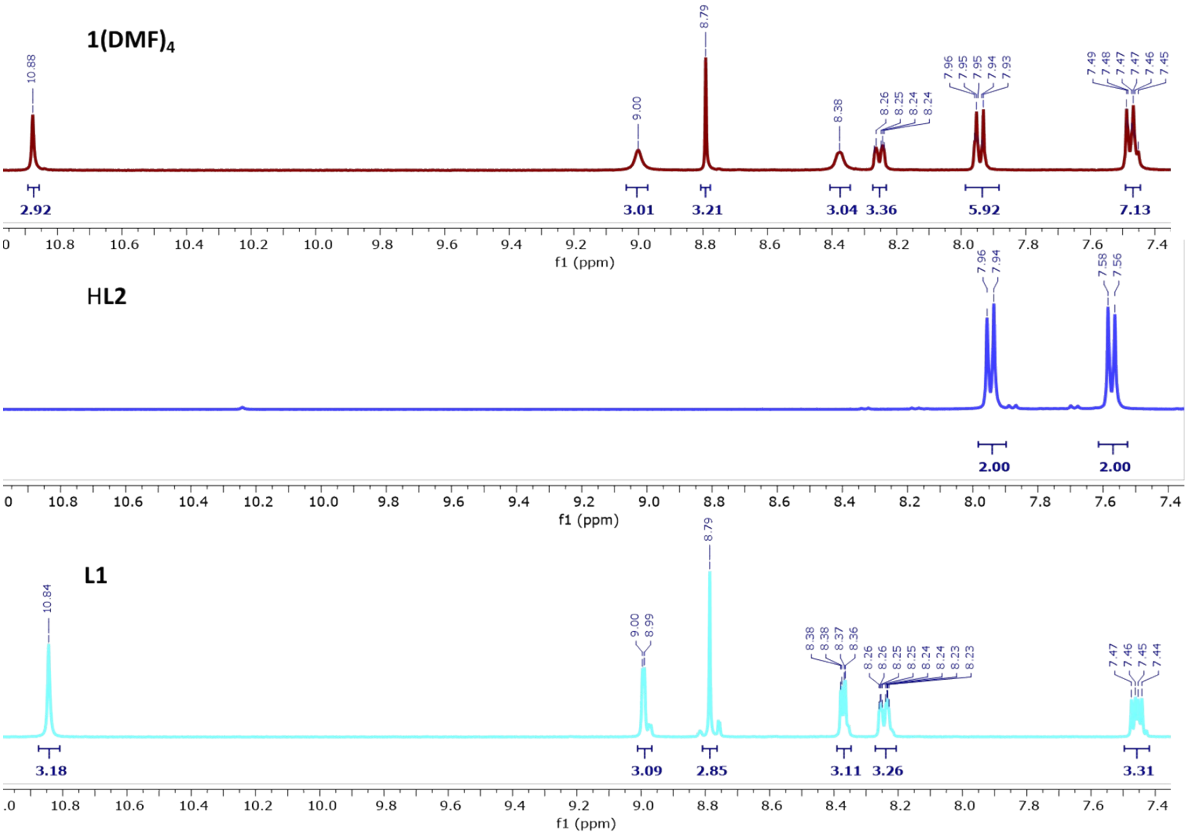

Figure S5. Comparison of ^{1}H-NMR (DMSO-d_6) spectra of **L1**, H**L2** and **1(DMF)$_4$**.

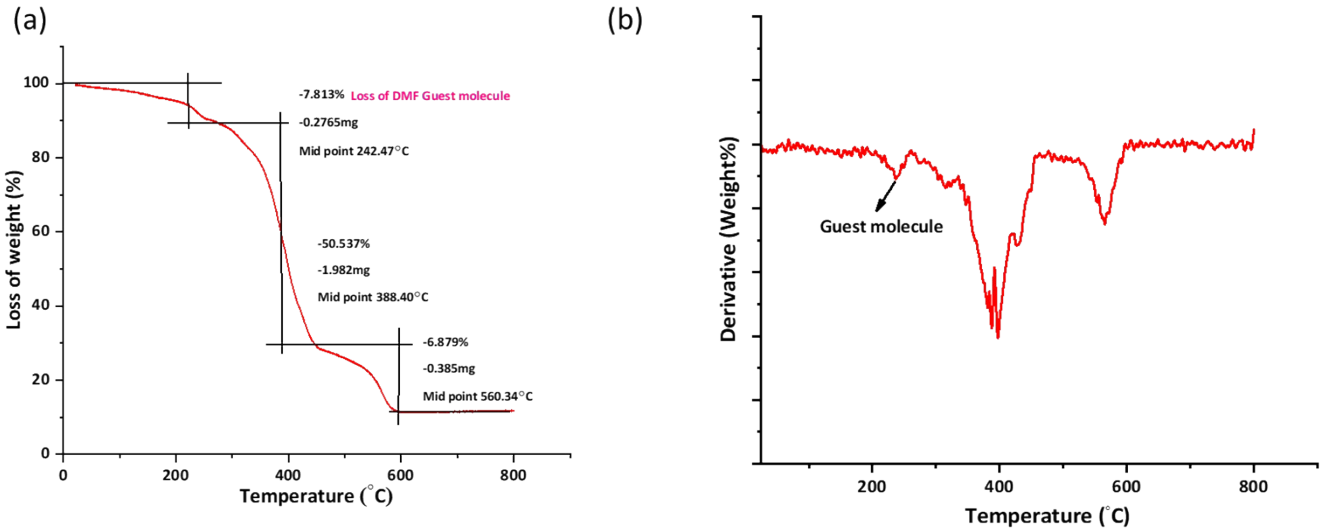

Figure S6. (a) TGA; (b) DTA-TG of **1(DMF)$_4$**.

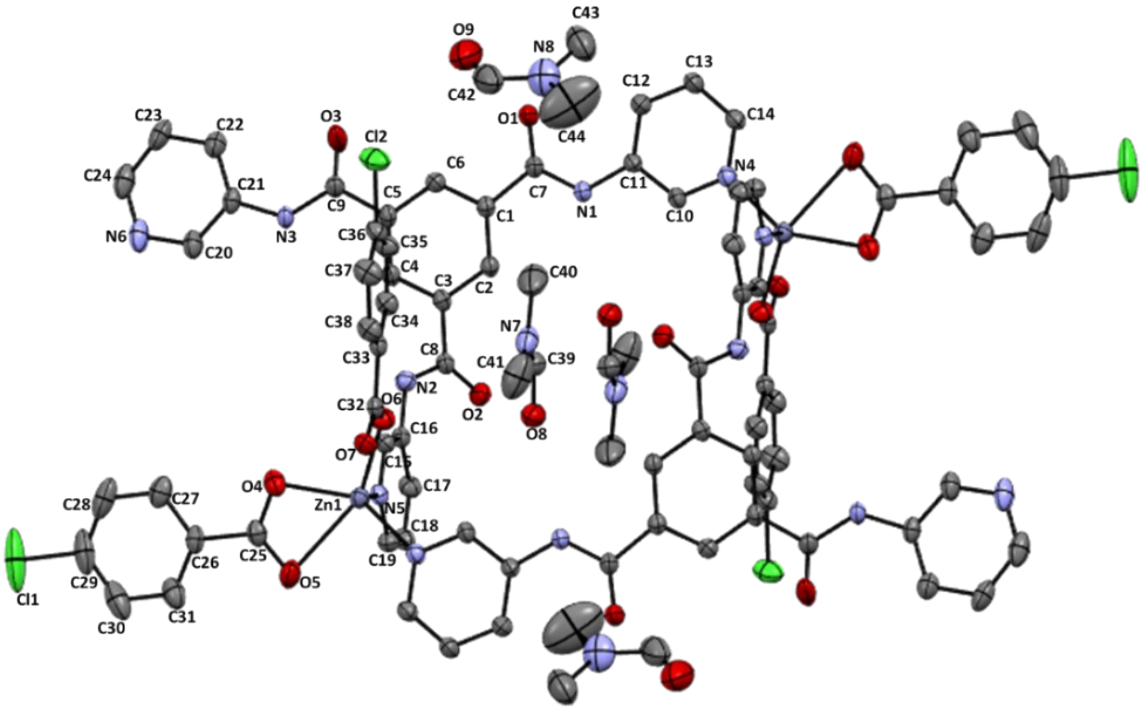

Figure S7. ORTEP of **1(DMF)$_4$** to show the atom numbering; Thermal ellipsoids shown at 50% probability (H atoms are not shown for clarity).

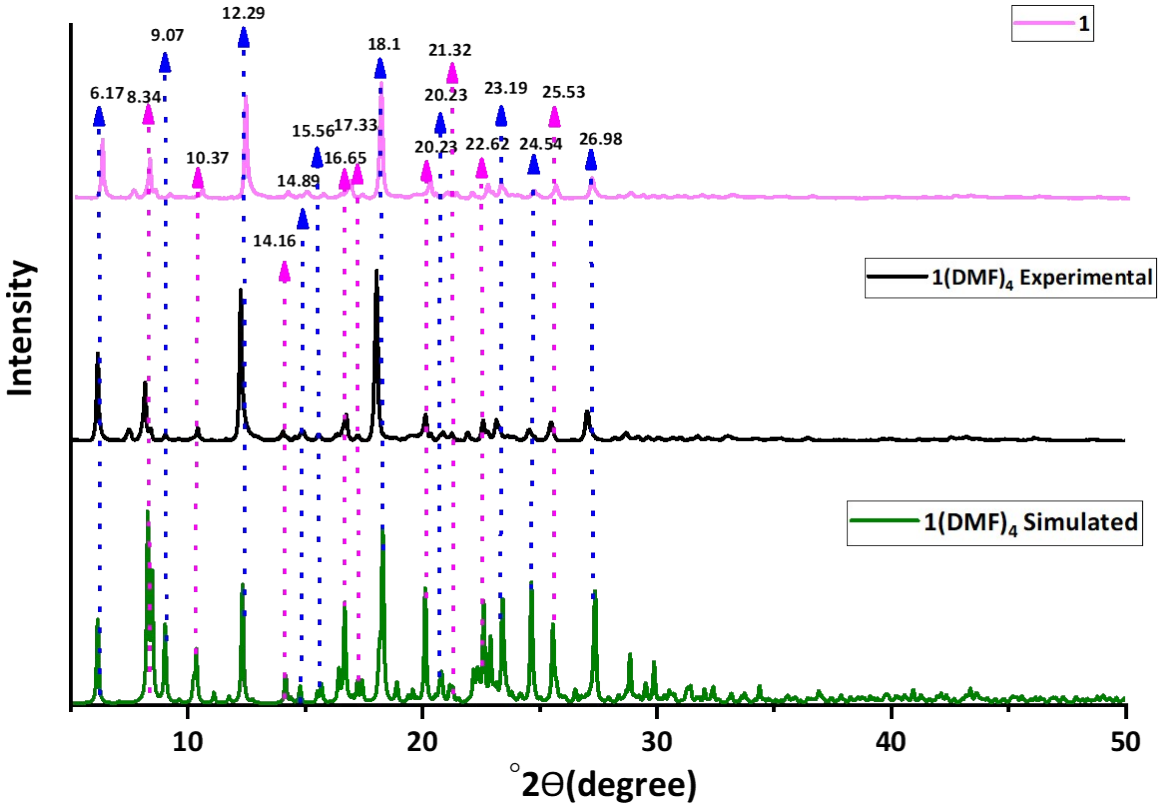

Figure S8. PXRD of **1(DMF)$_4$**: Simulated **1(DMF)$_4$**, Experimental **1(DMF)$_4$** and **1** (without DMF)

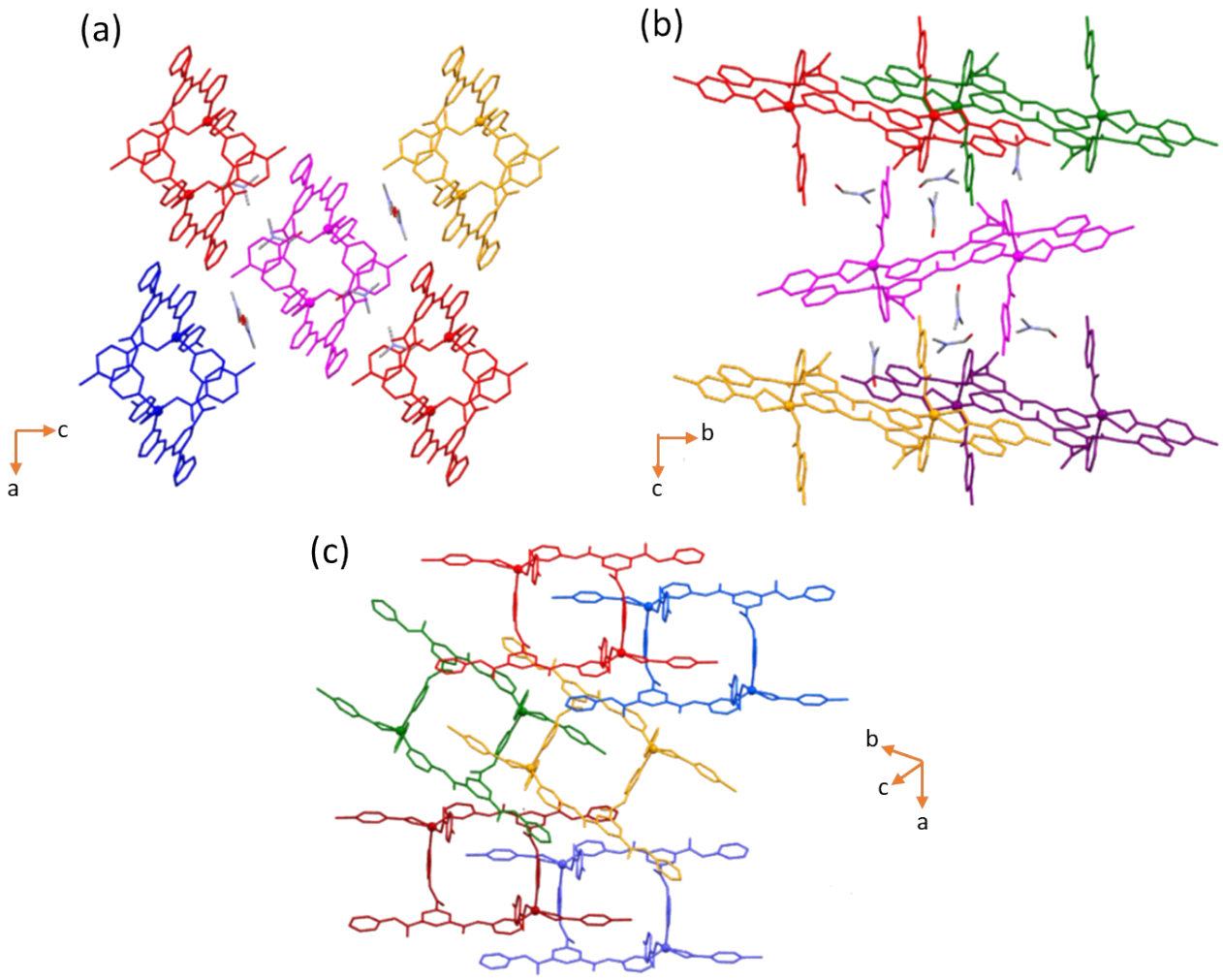

Figure S9. Packing of the rings in **1(DMF)$_4$**.

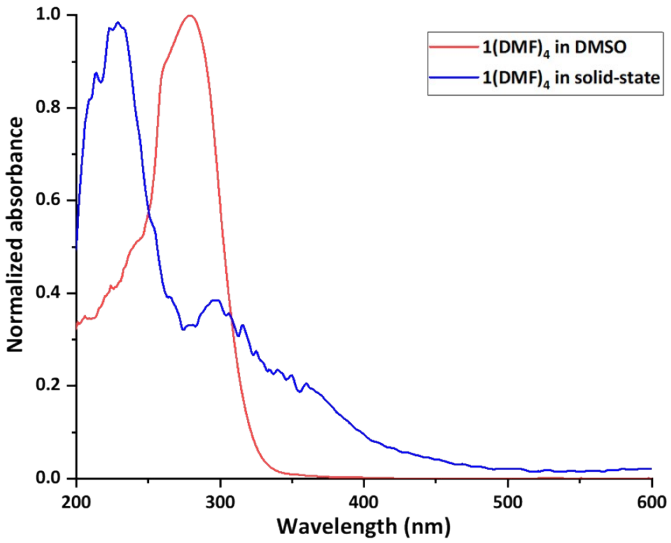

Figure S10. Normalized UV-Visible absorption spectra of **1(DMF)$_4$** in solid state and in DMSO (concentration = 1×10^{-5} M; λmax = 278 nm; ε = 38959 M^{-1} cm^{-1}; Concentration of **1(DMF)$_4$** is calculated by taking its asymmetric unit, molecular weight of 961.11).

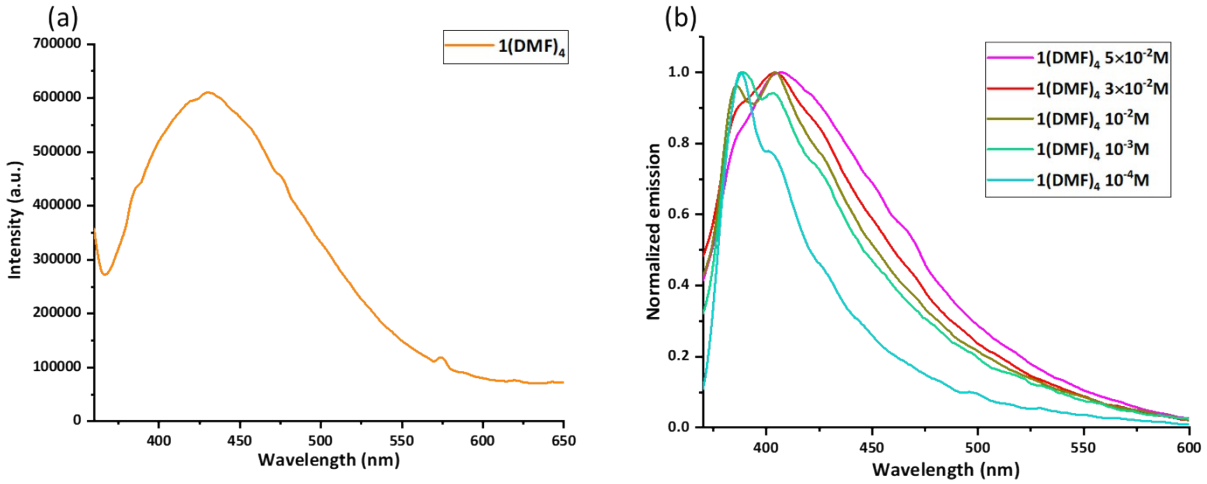

Figure S11. Photoluminescence spectra of **1(DMF)$_4$** (a) in solid-state and (Excitation wavelength = 350 nm, slit width = 2.5 nm) (b) in DMSO at different concentrations (Excitation wavelength = 350 nm, slit width = 4 nm) (Concentration of **1(DMF)$_4$** is calculated by taking its asymmetric unit, molecular weight of 961.11).

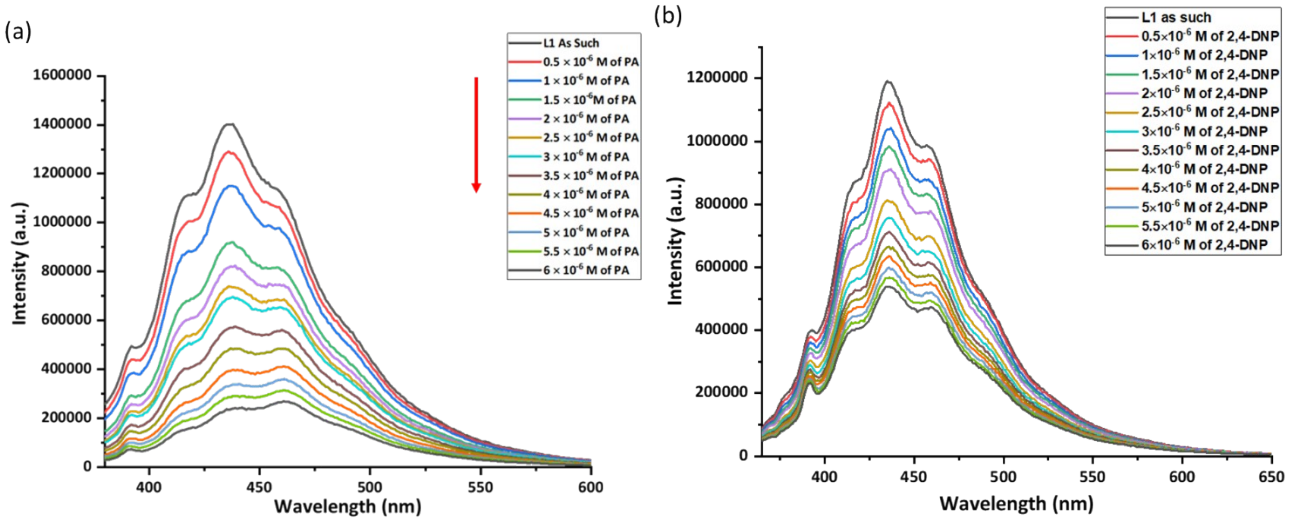

Figure S12. Fluorescence titrations of **L1** (10^{-2} M) DMSO with (a) PA (10^{-5}M) and (b) 2,4-DNP (10^{-5}M).

Note: For preparing the solution for each measurement, 100 µL DMSO solution of 10^{-5} M analyte (PA or 2,4-DNP) was added to 1.99 mL of 10^{-2} M solution of **L1** in DMSO to make a final volume of 2 mL. Similarly, other solutions were prepared by varying the concentration of the analyte and **1(DMF)$_4$** while maintaining the final volume to 2 mL.

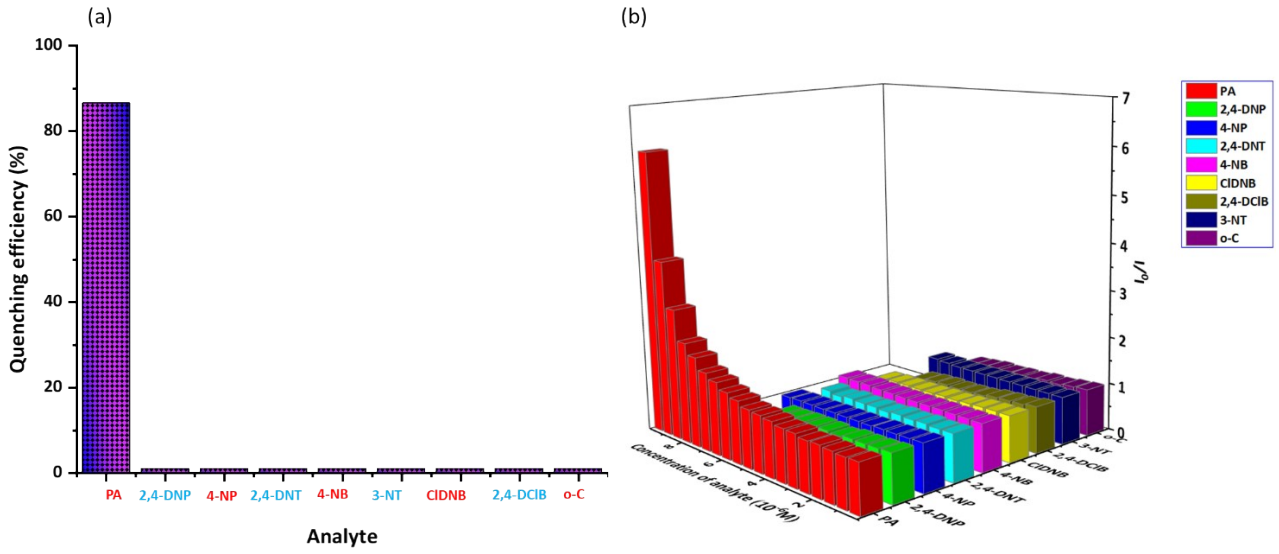

Figure S13. (a) Fluorescence quenching percentages of **1(DMF)$_4$** (in DMSO) in presence of different aromatic compounds; (b) S-V plot of **1(DMF)$_4$** (in DMSO) in presence of different aromatic compounds.

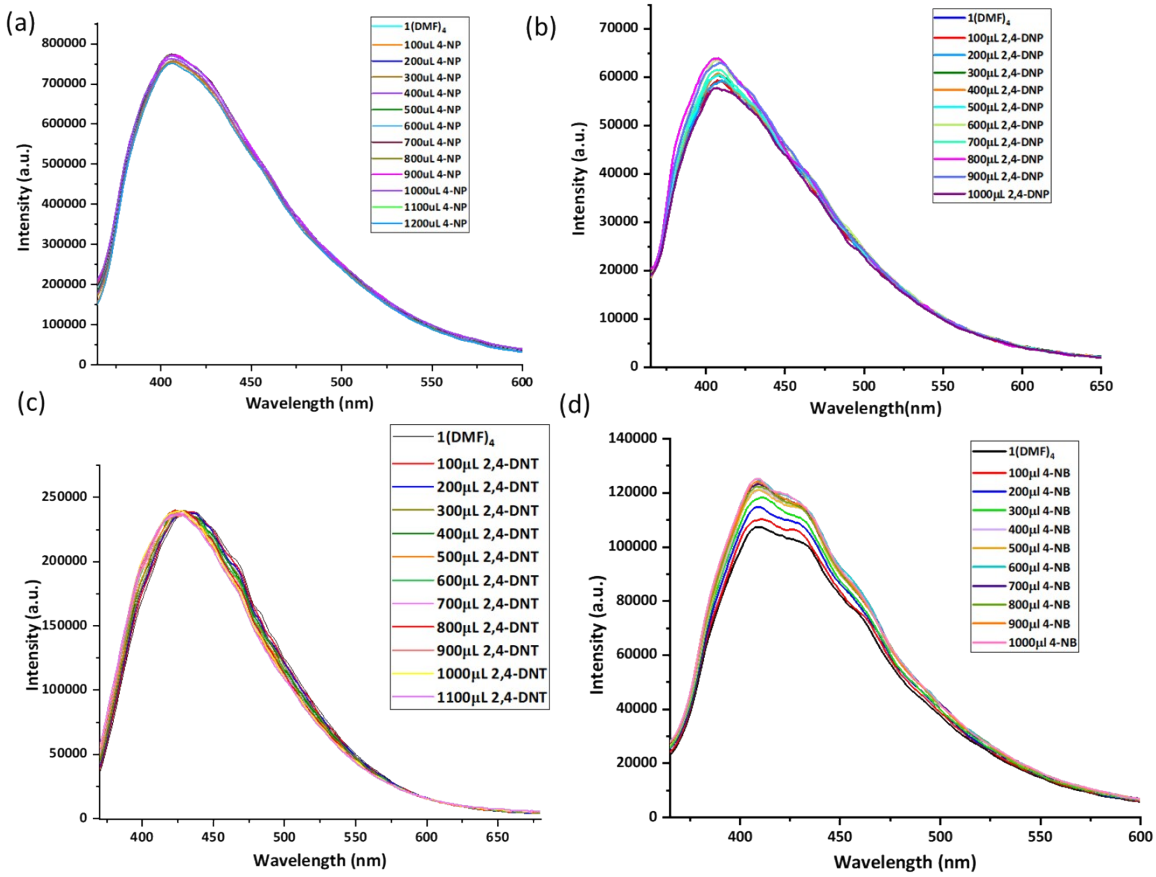

Figure S14. Fluorescence quenching titrations of **1(DMF)$_4$** in DMSO with (a) 4-NP; (b) 2,4-DNP; (c) 2,4-DNT; (d) 4-NB**.**

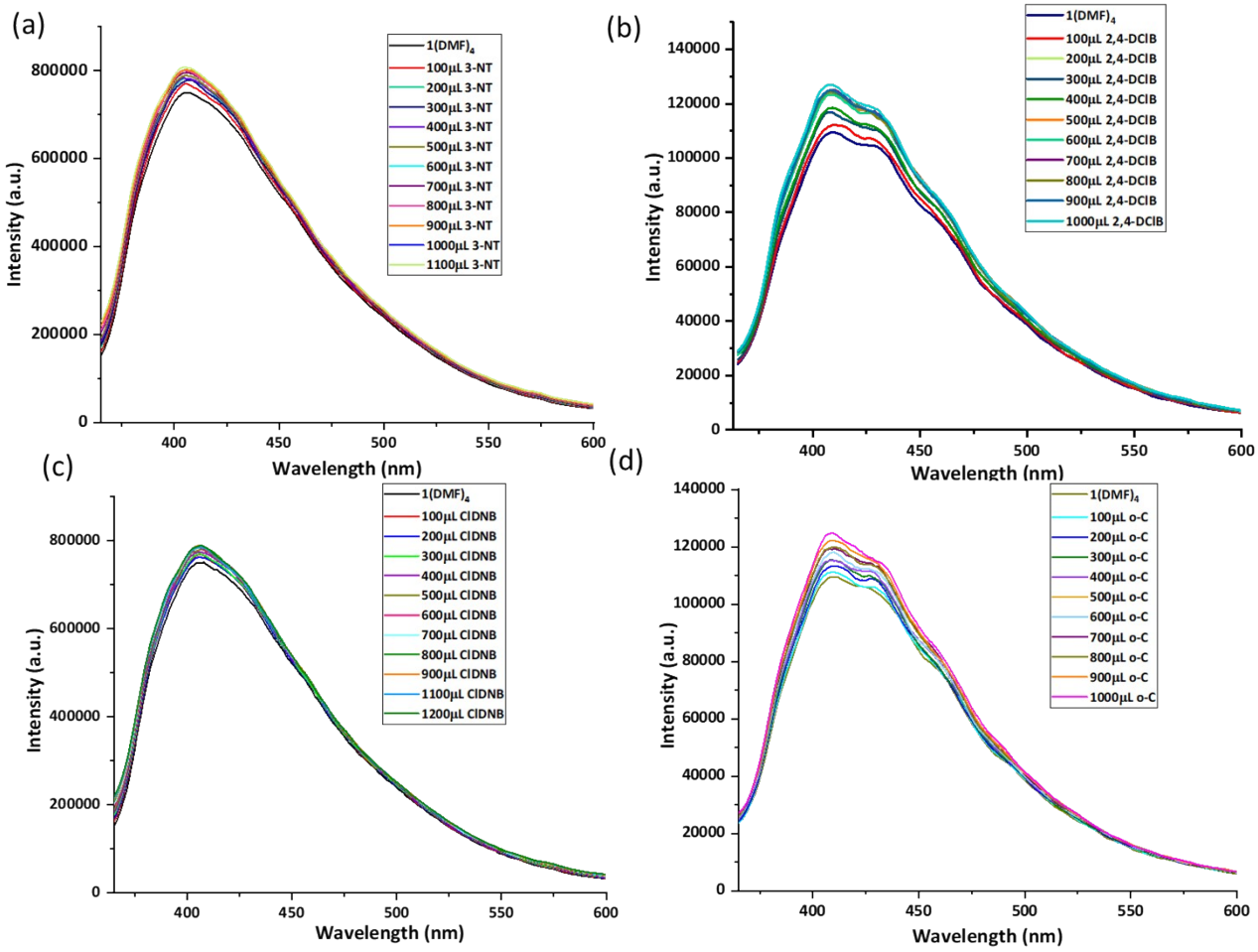

Figure S15. Fluorescence quenching titrations of **1(DMF)$_4$** in DMSO with (a) 3-NT; (b) 2,4-DClB (c) ClDNB (d) o-C.

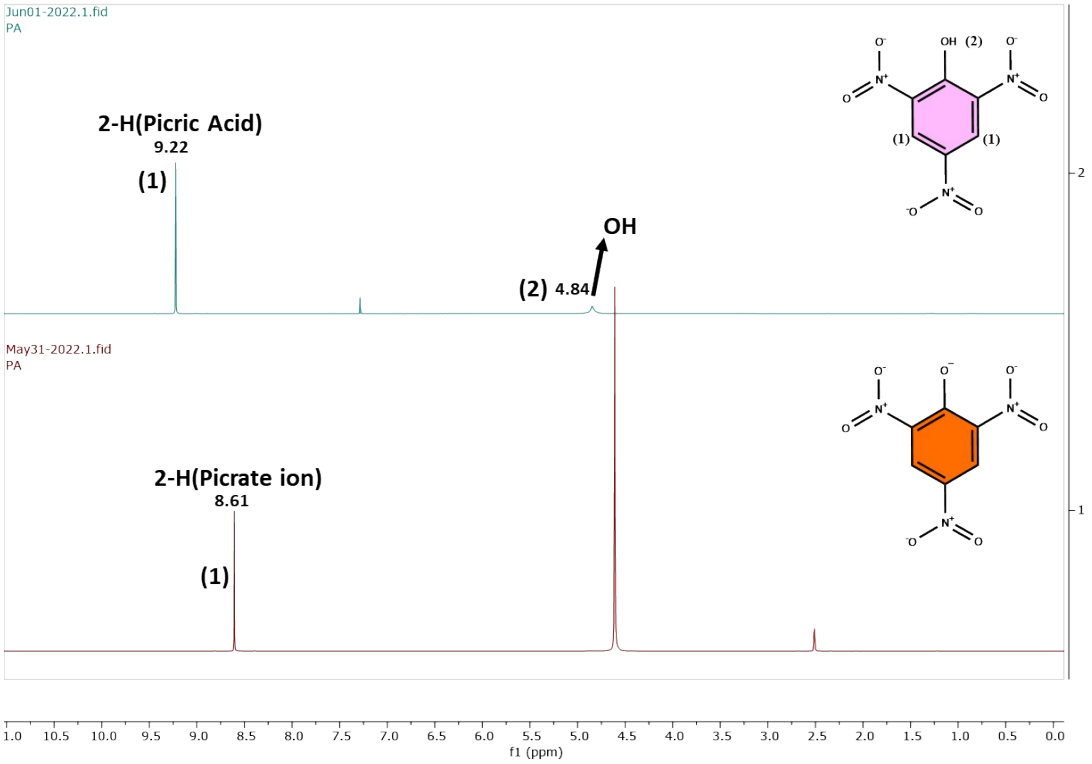

Figure S16. ^{1}H-NMR of PA in $CDCl_3$ and in DMSO-d_6.

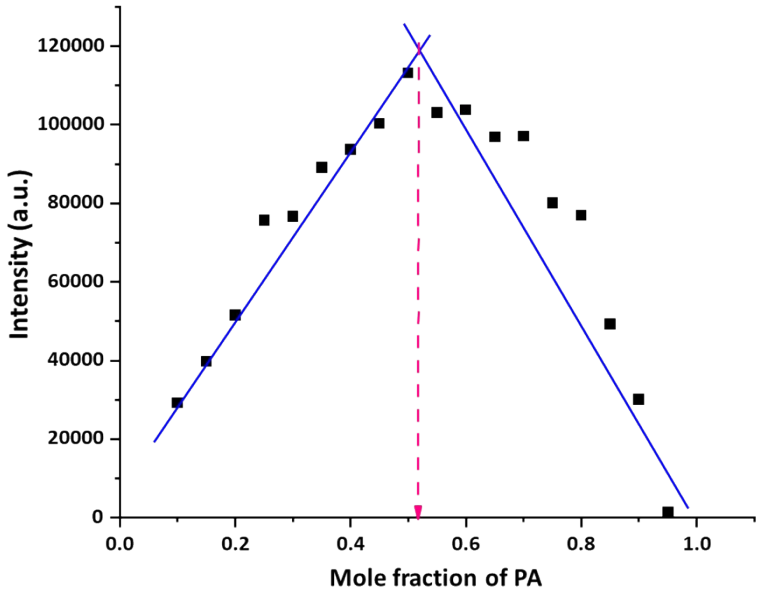

Figure S17. Jobs plot for estimating the binding ratio of **1(DMF)$_4$** and PA in DMSO.

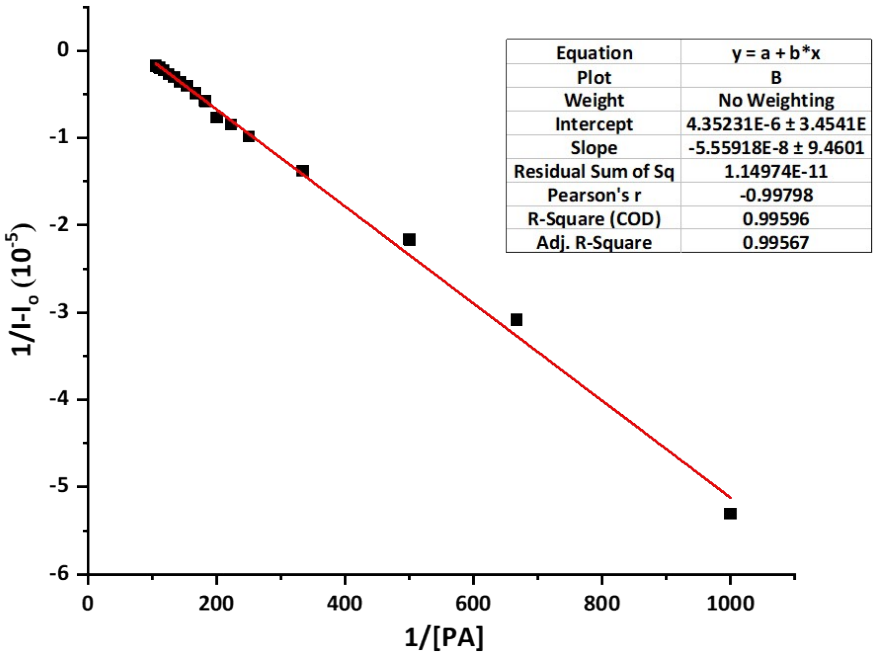

Figure S18. Benesi–Hildebrand (B-H) plot for determination of binding constant of **1(DMF)$_4$** and PA in DMSO.

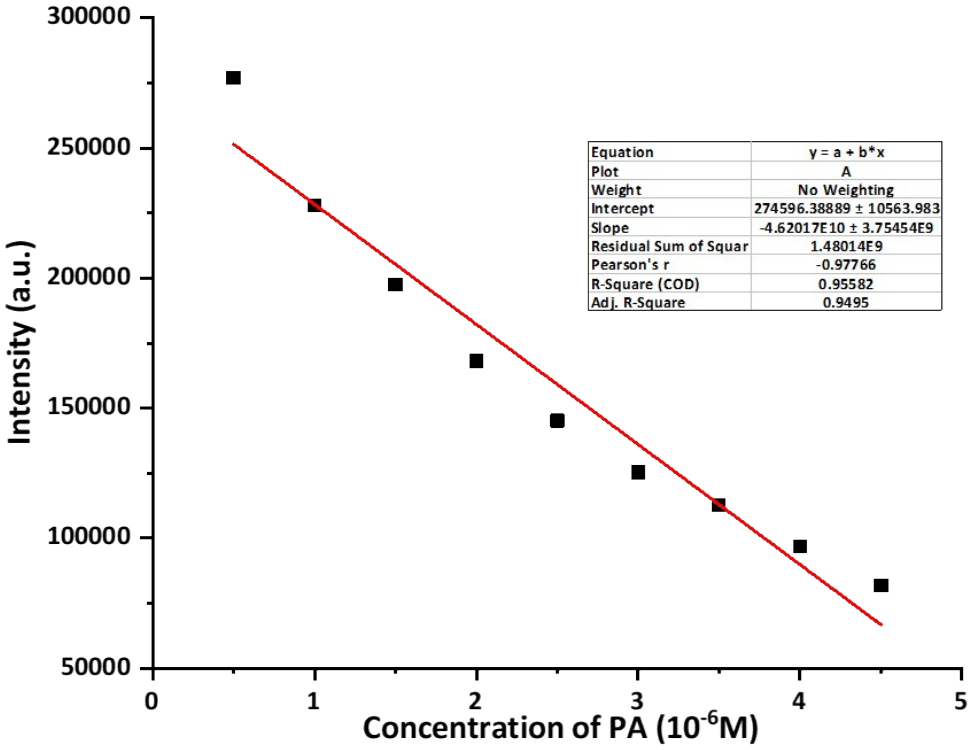

Figure S19. Plot of fluorescene intensity at 410 nm Vs. concentration of PA in DMSO (σ = 1.054).

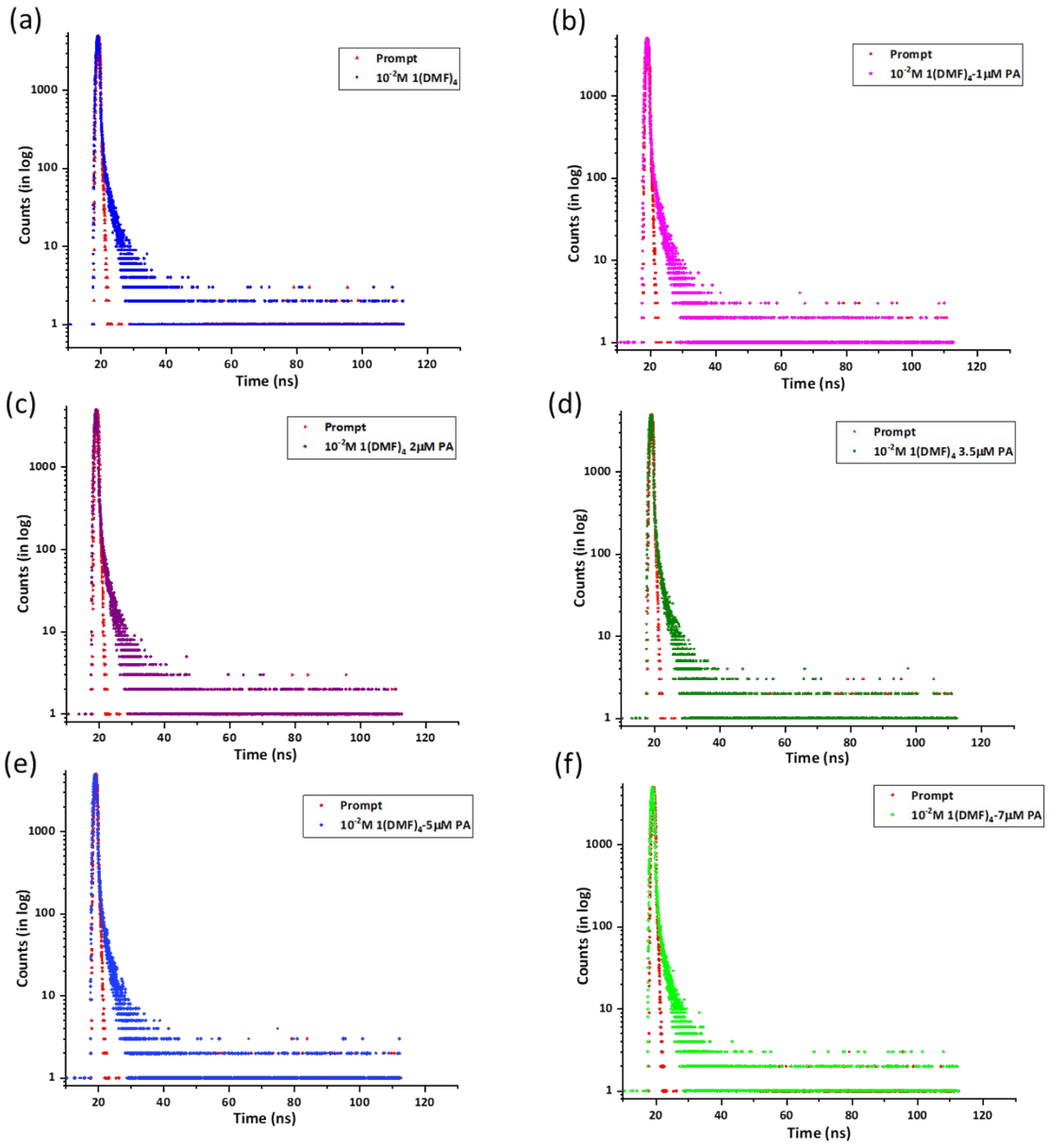

Figure S20. Time-resolved fluorescence decay profiles (Excitation wavelength = 350nm) in DMSO: (a) **1(DMF)$_4$** (Concentration = 10^{-2}M); (b) **1(DMF)$_4$** (Concentration = 10^{-2}M) and PA (Concentration= 1μM); (c) **1(DMF)$_4$** (Concentration = 10^{-2}M) and PA (Concentration = 2μM); (d) **1(DMF)$_4$** (Concentration =10^{-2}M) and PA (Concentration = 3.5μM); (e) **1(DMF)$_4$** (Concentration =10^{-2}M) and PA (Concentration = 5μM); (f) **1(DMF)$_4$** (Concentration =10^{-2}M) and PA (Concentration = 7μM).

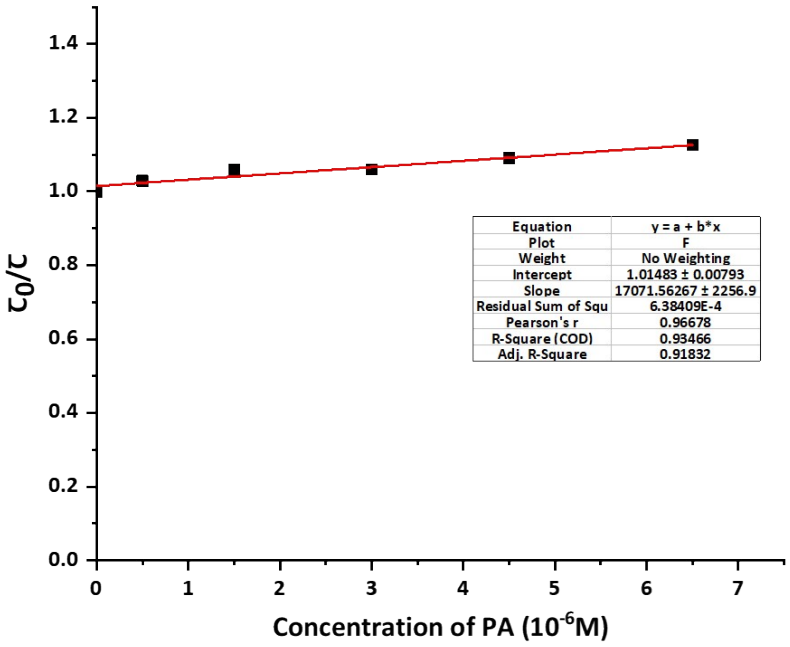

Figure S21. Plot of τ_0/τ Vs. Concentration of PA (Analyte/Quencher); The plot verifies the presence of static quenching.

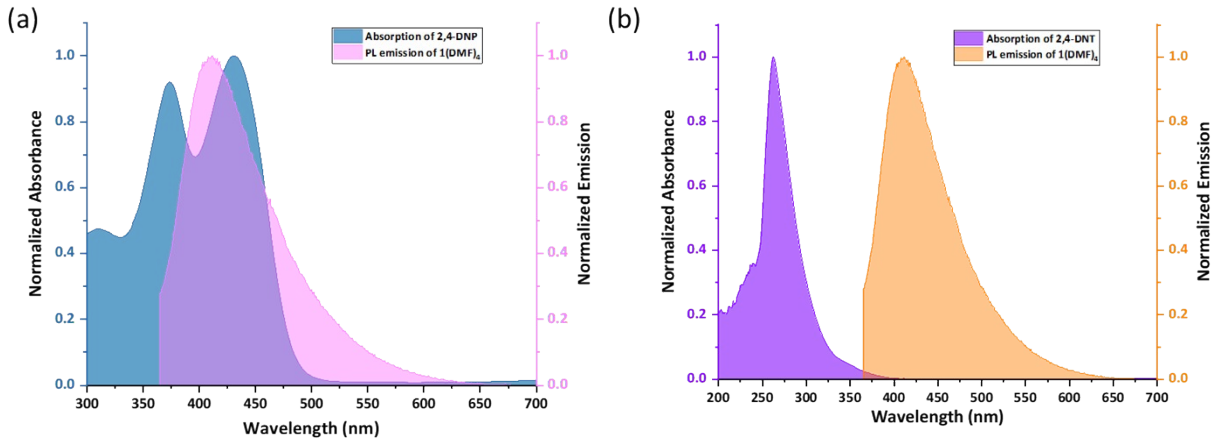

Figure S22. Overlap of emission spectrum of **1(DMF)$_4$** in DMSO with absorption spectrum of (a) 2,4-DNP (Overlap integral of **1(DMF)$_4$** and 2,4-DNP J (λ) = 7.37 × 10^{14} $M^{-1}cm^{-1}nm^4$ R_o = 18.85 Å) (b) 2,4-DNT (Overlap integral of **1(DMF)$_4$** and J (λ) = 2.92 × 10^{12} $M^{-1}cm^{-1}nm^4$, R_o = 7.50 Å).

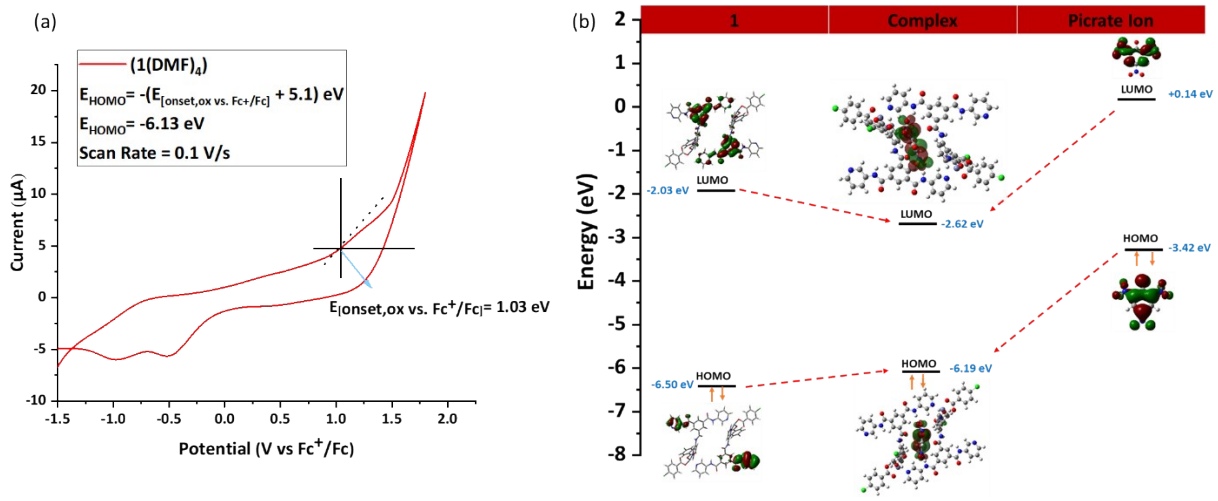

Figure S23 (a) Cyclic voltametric analysis of **1(DMF)$_4$** in DMSO (10^{-3}M); (b) HOMO and LUMO energies for **1** (in DMSO) and picrate ion estimated from DFT.

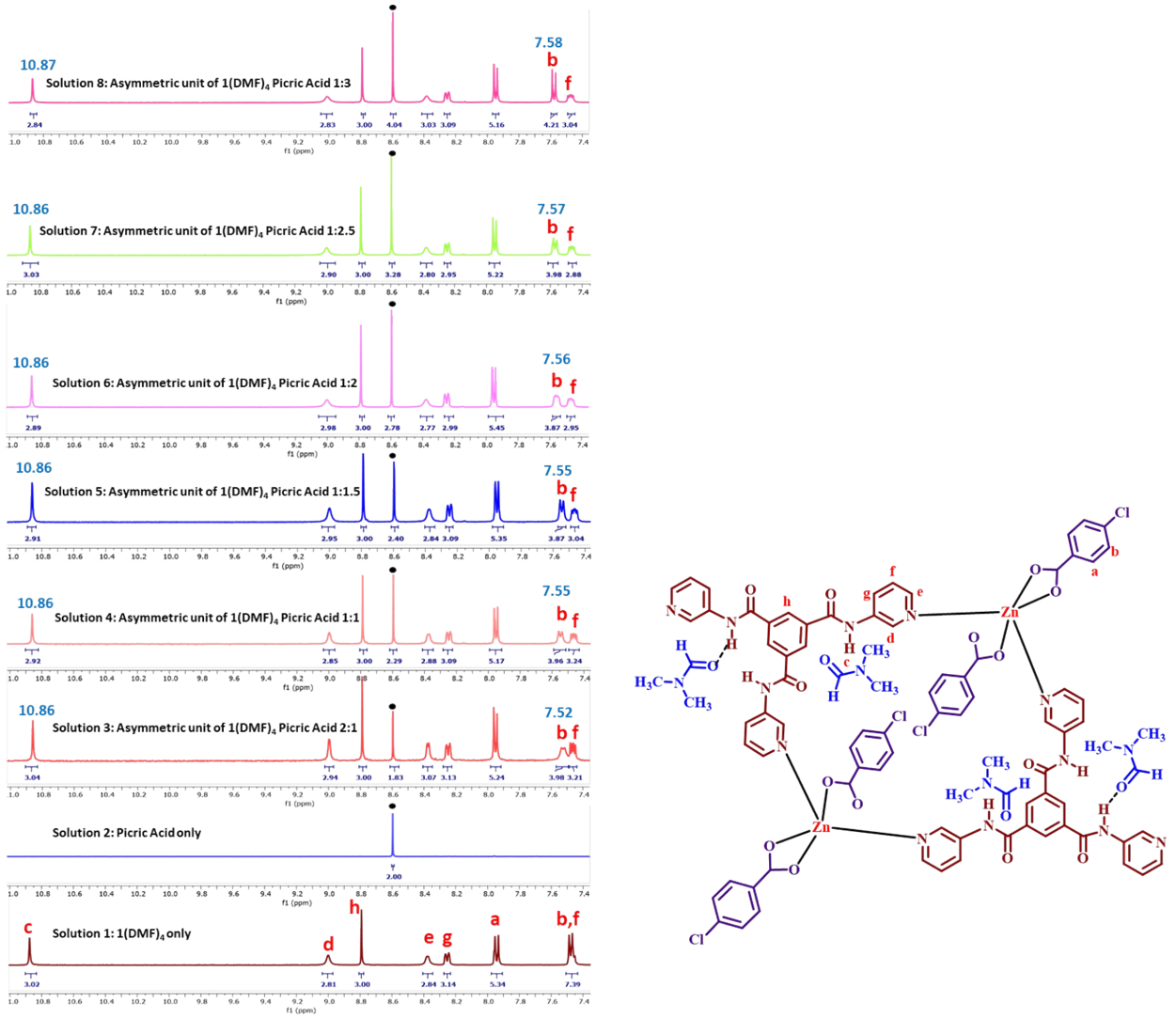

Figure S24. ^{1}H-NMR spectra of different ratio of **1(DMF)$_4$** (14.59 mM in DMSO-d$_6$) and PA (14.59 mM in DMSO-d$_6$): Solution 1: 0.10 mL of **1(DMF)$_4$** + 0.30 mL of DMSO-d$_6$; Solution 2: 0.1 mL of PA + 0.3 mL of DMSO-d$_6$; Solution 3: 0.1 mL of **1(DMF)$_4$** + 0.05 mL of PA + 0.25 mL of DMSO-d$_6$; Solution 4: 0.1 mL of **1(DMF)$_4$** + 0.1 mL of PA + 0.2 mL of DMSO-d$_6$; Solution 5: 0.1 mL of **1(DMF)$_4$** + 0.15 mL of PA + 0.15 mL of DMSO-d$_6$; Solution 6: 0.1 mL of **1(DMF)$_4$** + 0.2 mL of PA + 0.1 mL of DMSO-d$_6$; Solution 7: 0.1 mL of **1(DMF)$_4$** + 0.25 mL of PA + 0.05 mL of DMSO-d$_6$; Solution 8: 0.1 mL of **1(DMF)$_4$** + 0.3 mL of PA. (Ratio of asymmetric unit of **1(DMF)$_4$**: PA is mentioned in each spectrum); (Concentration of **1(DMF)$_4$** is calculated by taking its asymmetric unit, molecular weight of 961.11; Note that PA in DMSO gets deprotonated to form picrate anion).

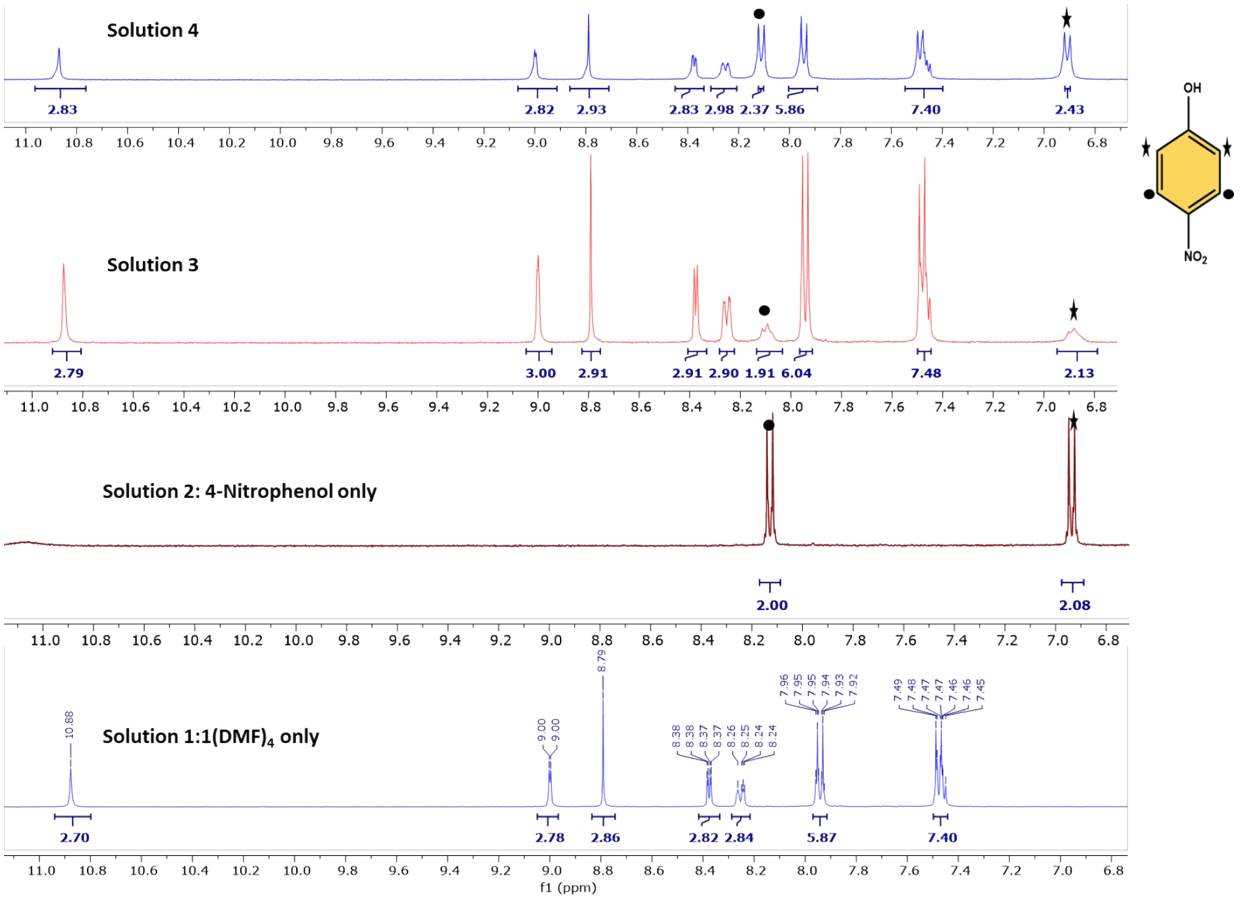

Figure S25. ^{1}H-NMR spectra of **1(DMF)$_4$** in DMSO-d$_6$ in presence of 4-NP: Solution 1: only **1(DMF)$_4$** (0.10 mL of 14.59 mM in DMSO-d$_6$) + 0.30 mL of DMSO-d$_6$; Solution 2: 4-NP (0.10 mL of 14.59 mM in DMSO-d$_6$) + 0.30 mL of DMSO-d$_6$; Solution 3: **1(DMF)$_4$** (0.10 mL of 14.59 mM in DMSO-d$_6$) + NP (0.05 mL of 14.59 mM in DMSO-d$_6$) +0.25 mL of DMSO-d$_6$; Solution 4: **1(DMF)$_4$** (0.10 mL of 14.59 mM in DMSO-d$_6$) + NP (0.25 mL of 14.59 mM in DMSO-d$_6$) +0.05 mL of DMSO-d$_6$. (Concentration of **1(DMF)$_4$** is calculated by taking its asymmetric unit, molecular weight of 961.11).

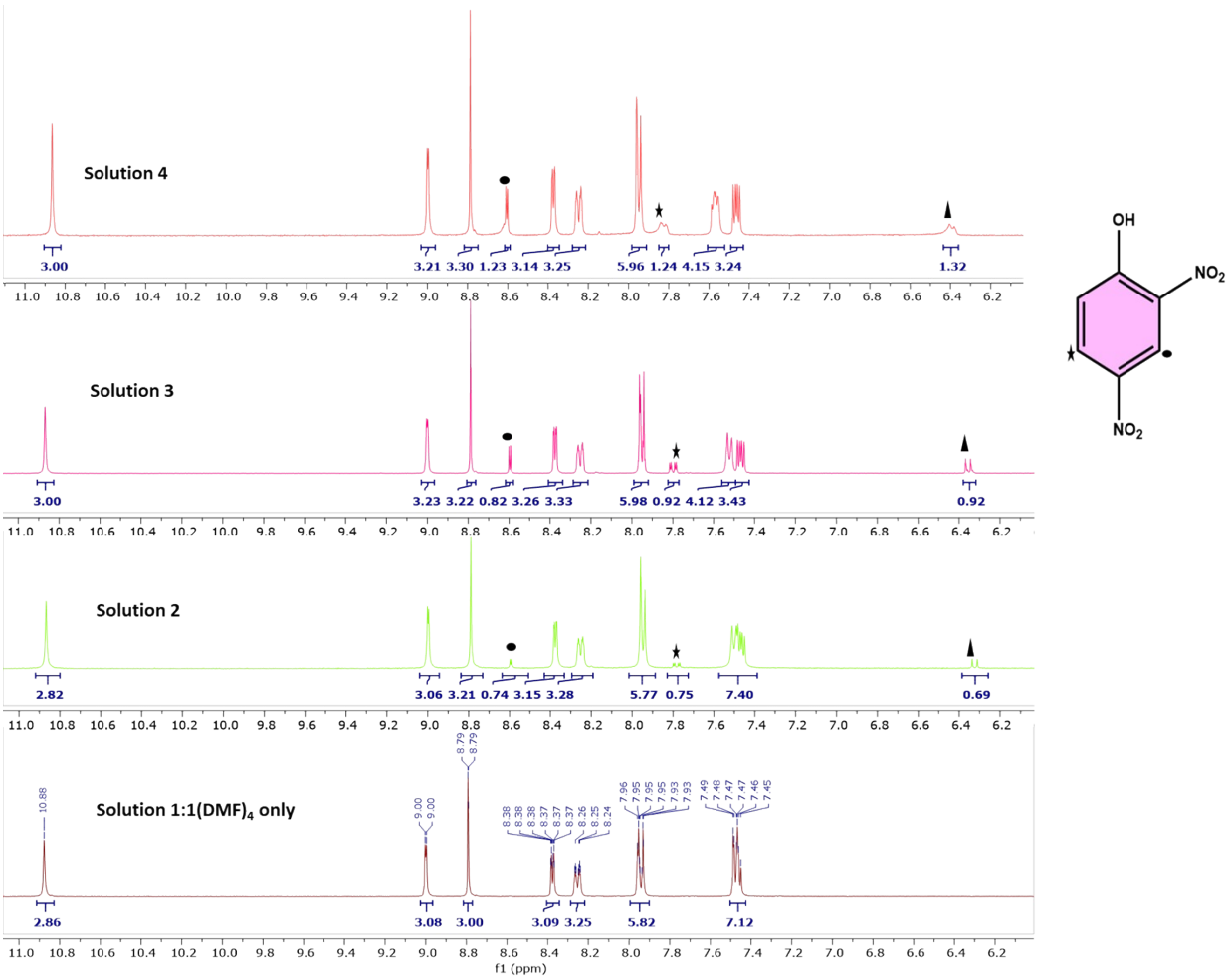

Figure S26. ^{1}H-NMR spectra of **1(DMF)$_4$** in DMSO-d6 in presence of 2,4-DNP: Solution 1: only **1(DMF)$_4$** (0.10 mL of 14.59 mM in DMSO-d$_6$) + 0.30 mL of DMSO-d$_6$; Solution 2: **1(DMF)$_4$** (0.10 mL of 14.59 mM in DMSO-d$_6$) + 2,4-DNP (0.05 mL of 14.59 mM in DMSO-d$_6$) +0.25 mL of DMSO-d$_6$; Solution 3: **1(DMF)$_4$** (0.10 mL of 14.59 mM in DMSO-d$_6$) + 2,4-DNP (0.15 mL of 14.59 mM in DMSO-d$_6$) +0.15 mL of DMSO-d$_6$; Solution 4: **1(DMF)$_4$** (0.10 mL of 14.59 mM in DMSO-d$_6$) + 2,4-DNP (0.25 mL of 14.59 mM in DMSO-d$_6$) +0.05 mL of DMSO-d$_6$. (Concentration of **1(DMF)$_4$** is calculated by taking its asymmetric unit, molecular weight of 961.11).

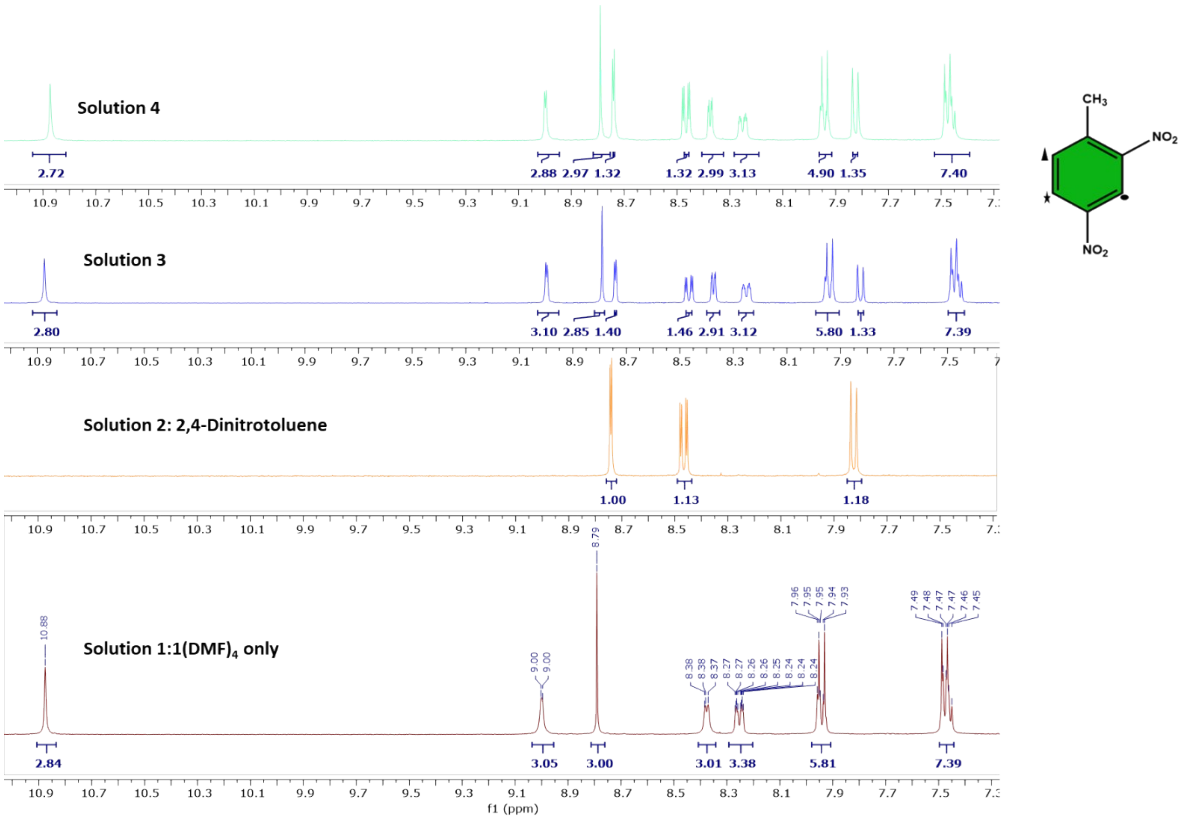

Figure S27. ^{1}H-NMR spectra of **1(DMF)$_4$** in DMSO-d$_6$ in presence of 2,4-DNT: Solution 1: only **1(DMF)$_4$** (0.10 mL of 14.59 mM in DMSO-d$_6$) + 0.30 mL of DMSO-d$_6$; Solution 2: only DNT (0.10 mL of 14.59 mM in DMSO-d$_6$) + 0.30 mL of DMSO-d$_6$; Solution 3: **1(DMF)$_4$** (0.10 mL of 14.59 mM in DMSO-d$_6$) + 2,4-DNT (0.20 mL of 14.59 mM in DMSO-d$_6$) +0.10 mL of DMSO-d$_6$; Solution 4: **1(DMF)$_4$** (0.10 mL of 14.59 mM in DMSO-d$_6$) + 2,4-DNT (0.30 mL of 14.59 mM in DMSO-d$_6$). (Concentration of **1(DMF)$_4$** is calculated by taking its asymmetric unit, molecular weight of 961.11).

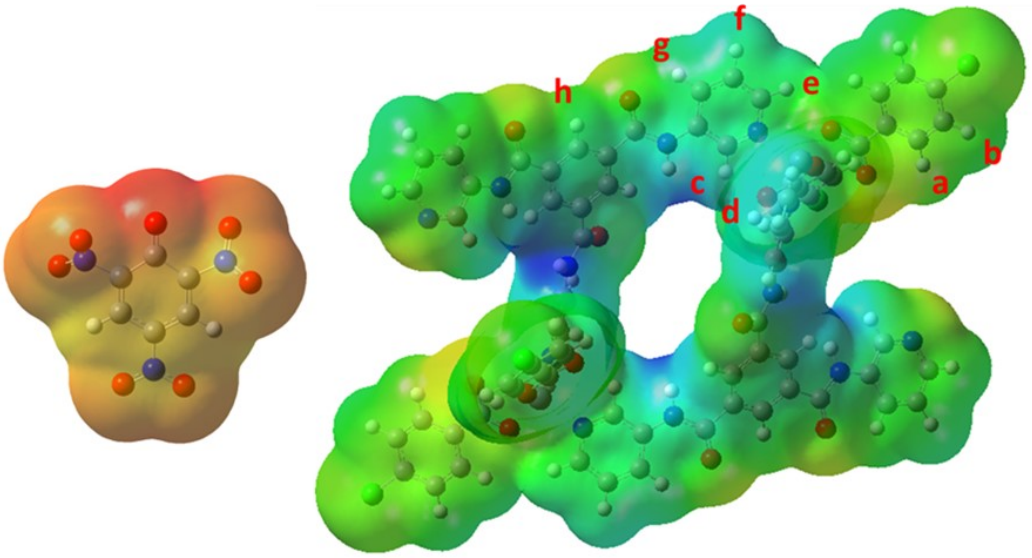

Figure S28. Electrostatic surface potentials of **1** (optimized in DMSO) and picrate which resulted in shifts in the peak position of N-Hc and Hb in ^{1}H-NMR.

.

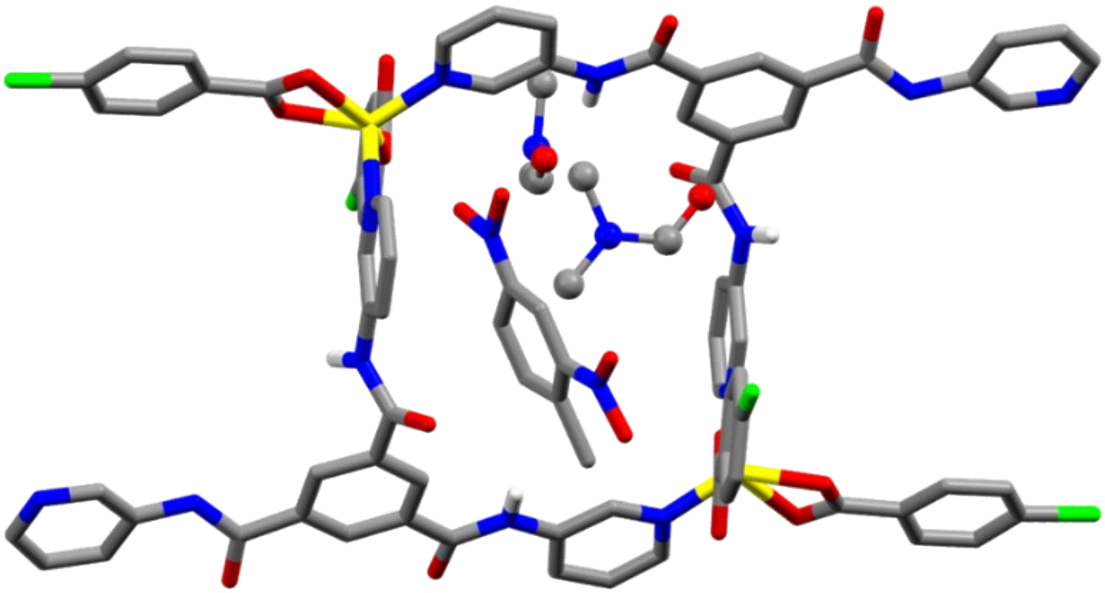

Figure S29. Molecular docking structure of **1(DMF)$_4$** and 2,4-DNT (DFT optimized geometry of the probe (in DMSO) and analyte were considered for docking studies).

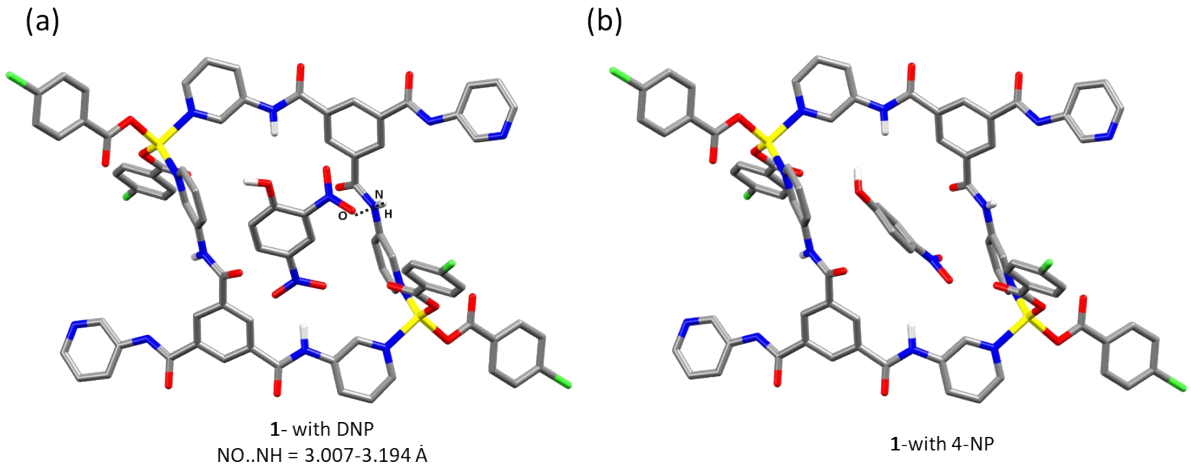

Figure S30. Molecular docking structure of **1** and other nitroaromatic compounds (2,4-DNP and 4-NP) (For the hydrogen bond interactions, the distances between the heteroatoms are mentioned, Interaction energy E = -176.1 kcal/mol between the **1**-in DMSO and 2,4-DNP). (Optimized geometry of the probe (in DMSO) and analyte were considered for docking studies).

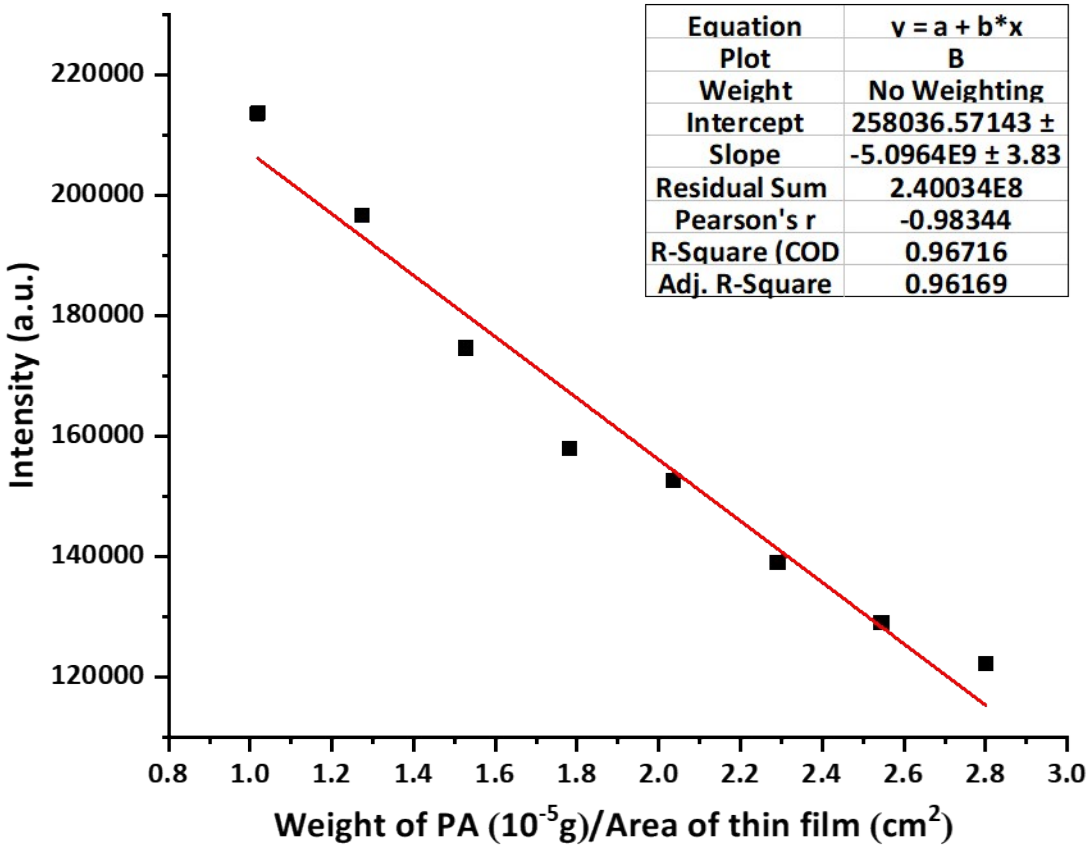

Figure S31. Plot of fluorescene intensity at 430 nm Vs. Weight of PA/Area of thin film on thin films of **1(DMF)$_4$** (σ = 0.8388).

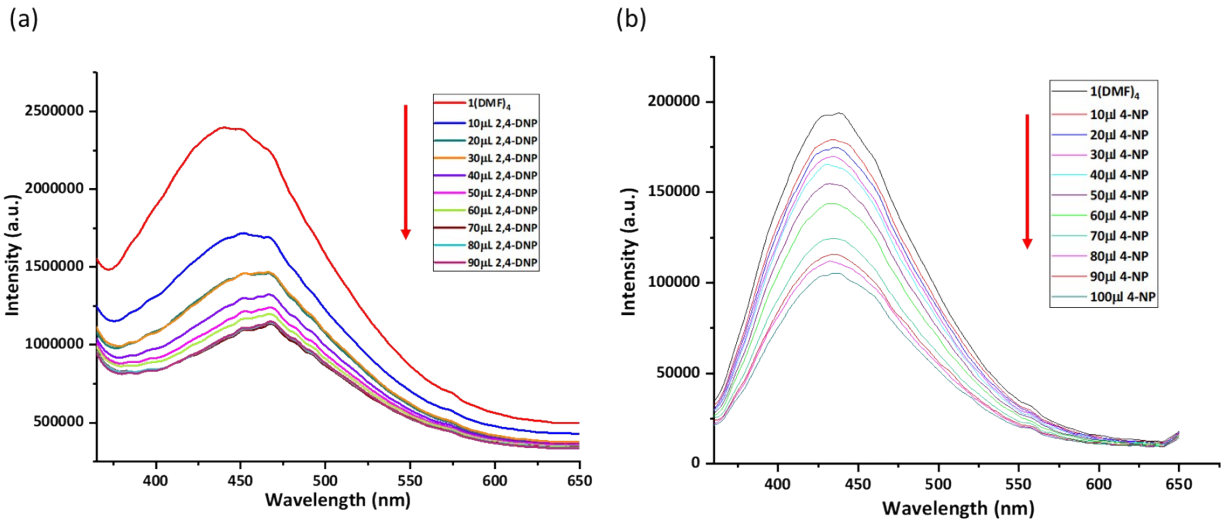

Figure S32. Fluorescence quenching titrations of thin films of **1(DMF)$_4$** with (a) 2,4-DNP and (b) 4-NP.

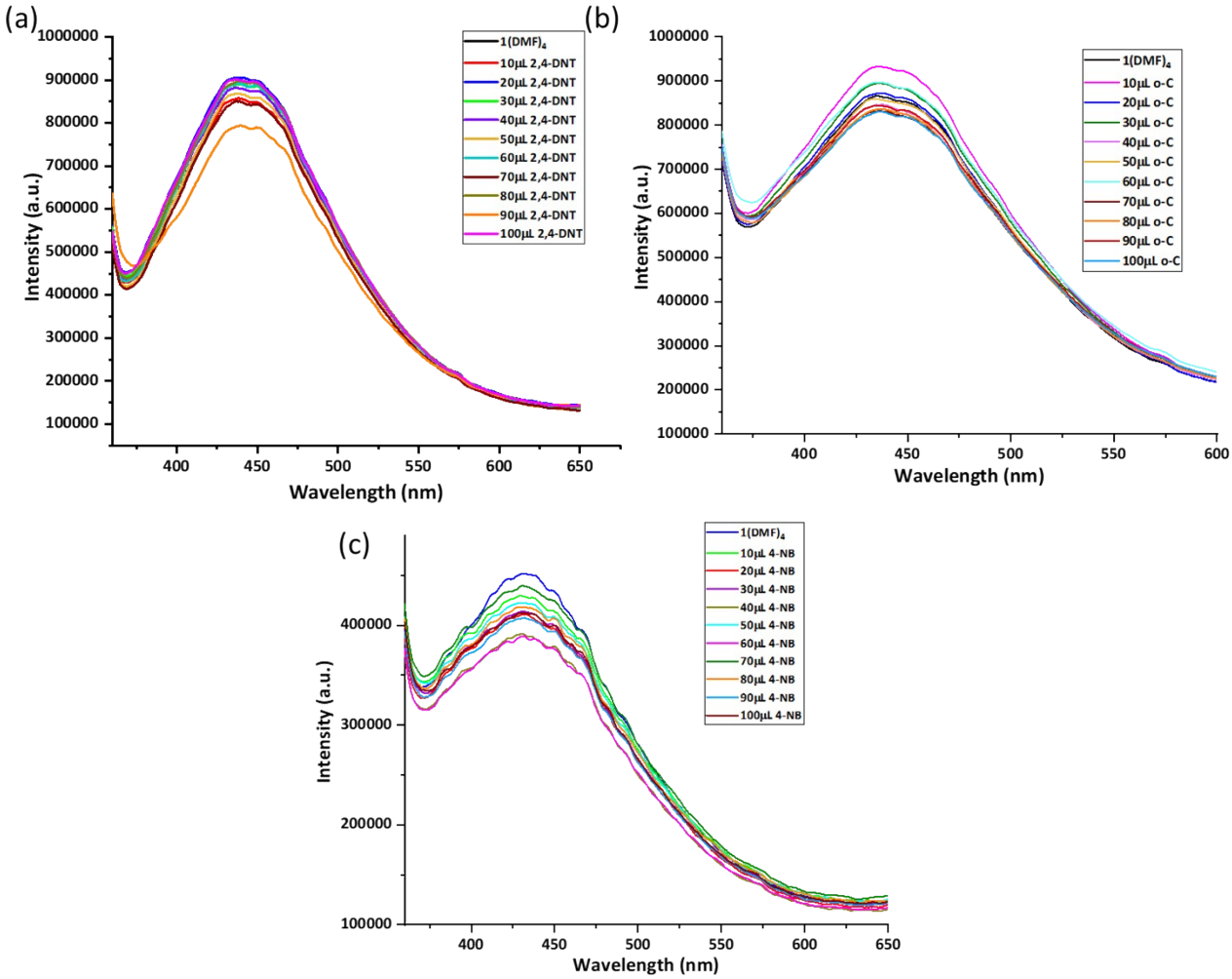

Figure S33. Fluorescence quenching titrations of thin films of **1(DMF)$_4$** with (a) 2,4-DNT and (b) o-C (c) 4-NB.

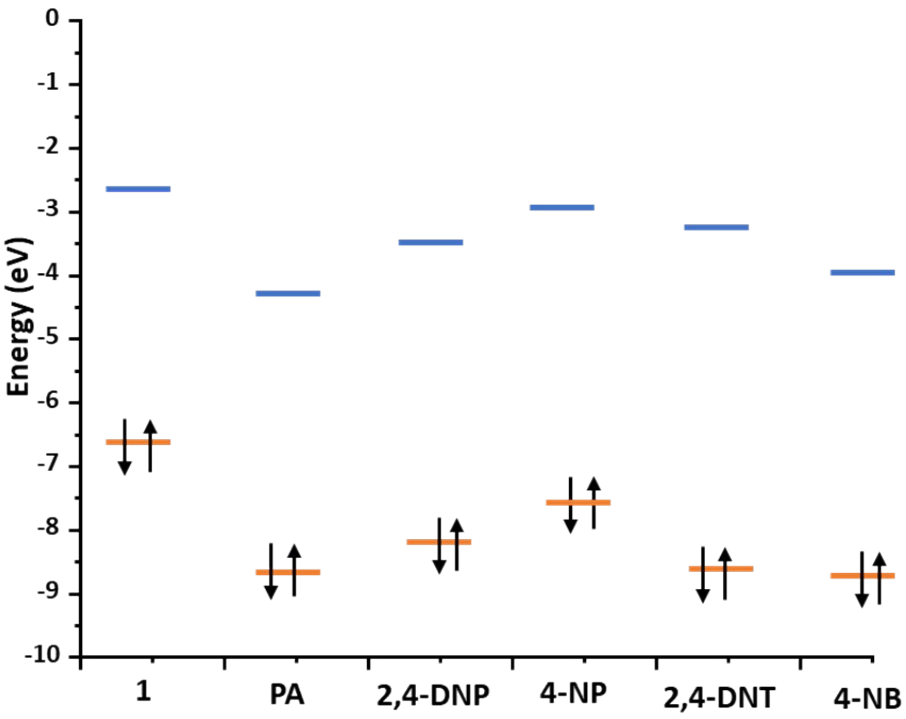

Figure S34. Frontier orbital diagrams of **1** and aromatic compounds PA, 2,4-DNP, 4-NP, 2,4- DNT, 4-NB.

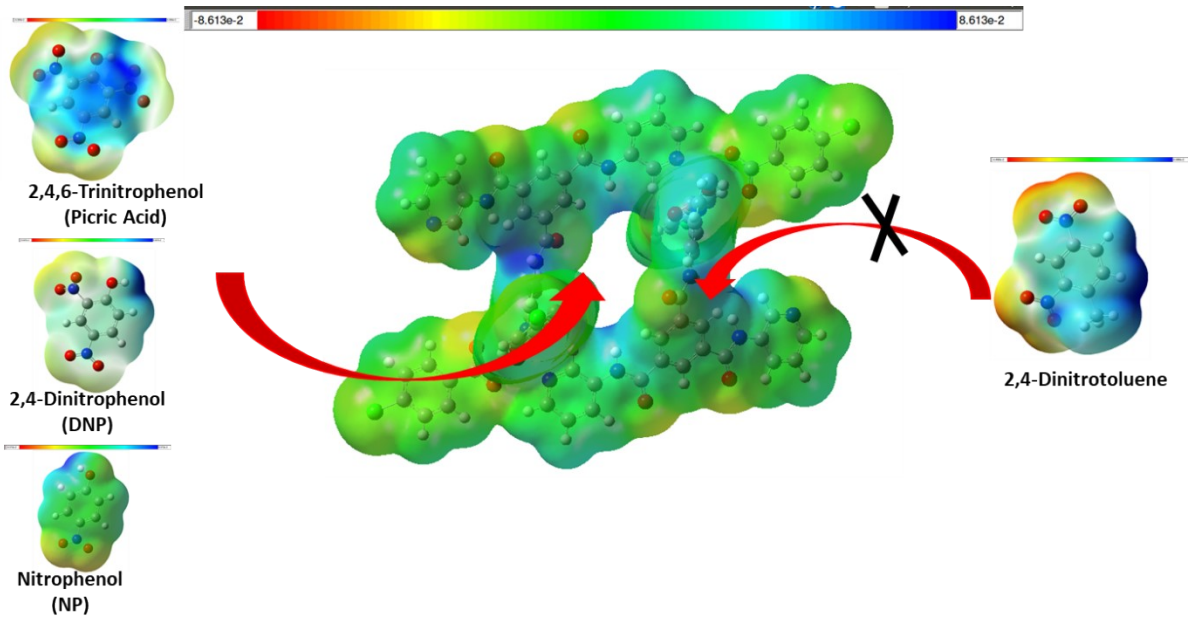

Figure S35. Electrostatic potential surfaces of **1** and aromatic compounds (Generated using the optimized geometry of **1**, where solvated DMF are removed before performing the optimization).

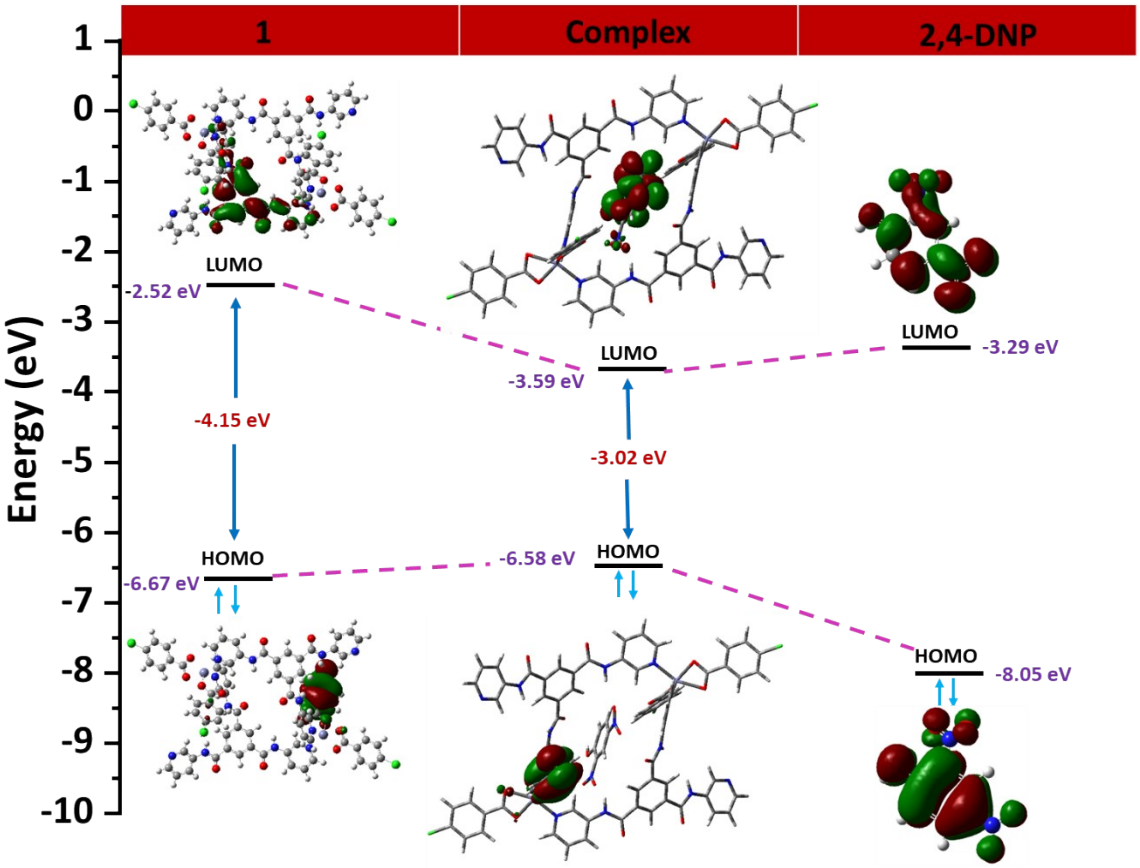

Figure S36. HOMO and LUMO energies for **1** and 2,4-DNP estimated from DFT.

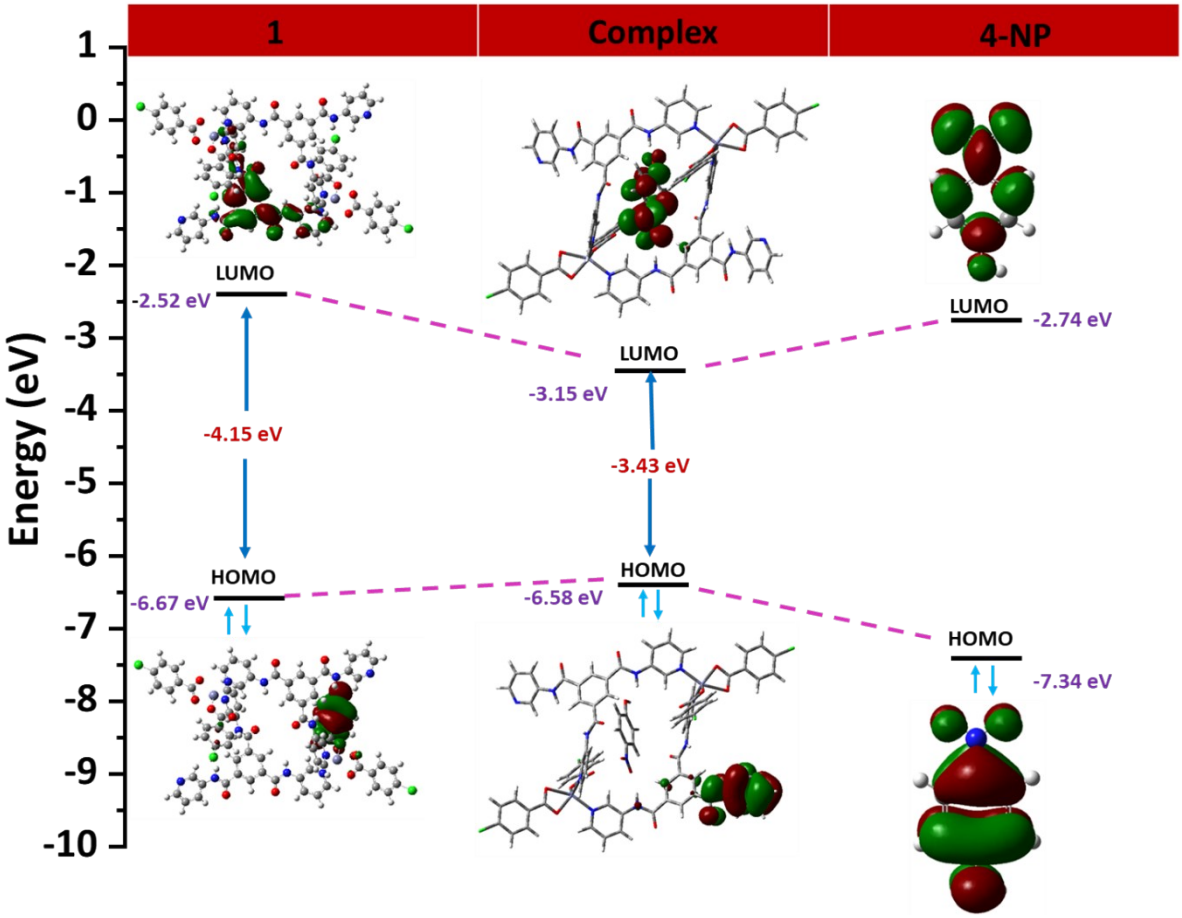

Figure S37. HOMO and LUMO energies for **1** and 4-NP estimated from DFT.

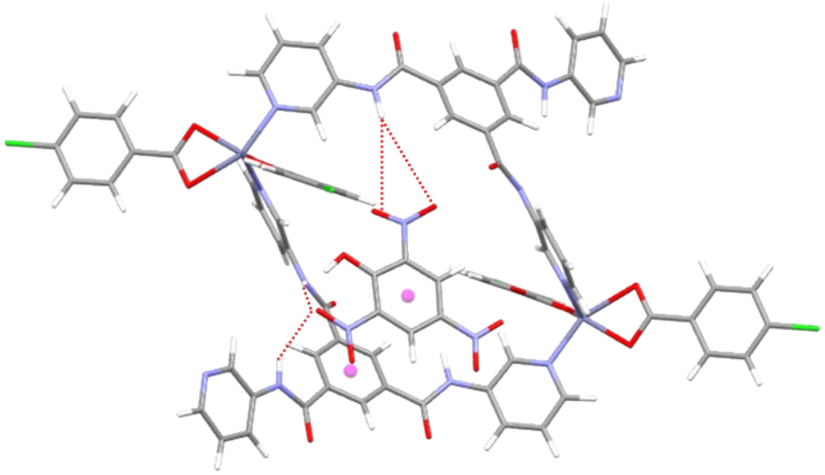

Figure S38. Molecular docking structure of **1**(optimised file of **1** with DFT is used) with PA.

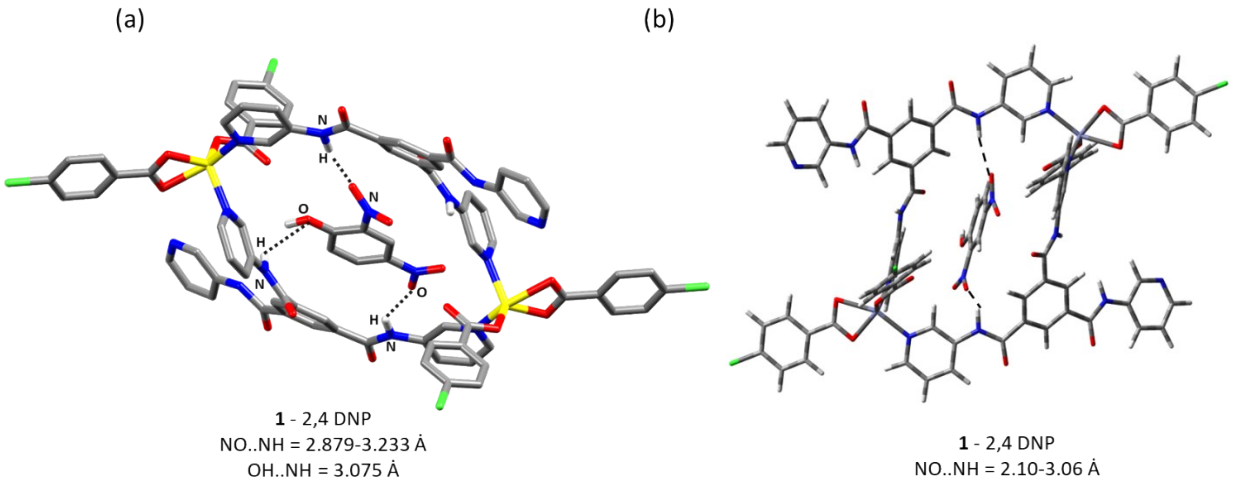

Figure S39. (a) Molecular docking structure of **1** (Optimized file of **1** by DFT is used) and 2,4-DNP; Interaction energy E= -185.1 kcal/mol; (b) Optimized Geometry of **1**-2,4-DNP along with possible interactions (dotted black line) obtained by DFT; Interaction energy = -120.51 kcal/mol (For the hydrogen bond interactions, the distances between the heteroatoms are mentioned, E is the energy of interaction between the probe and the analyte).

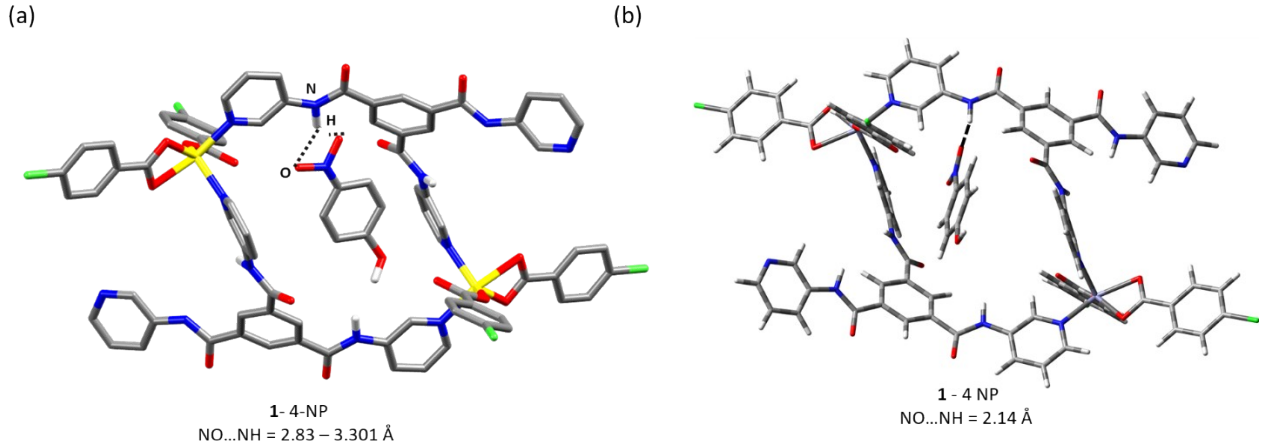

Figure S40. (a) Molecular docking structure of **1** (Optimized file of **1** by DFT is used) and 4-NP; Interaction energy E = -150.6kcal/mol; (b) Optimized Geometry of 1-4-NP along with possible interactions (dotted black line) obtained by DFT; Interaction energy E = -80.09 kcal/mol (For the hydrogen bond interactions, the distances between the heteroatoms are mentioned, E is the energy of interaction between the probe and the analyte).

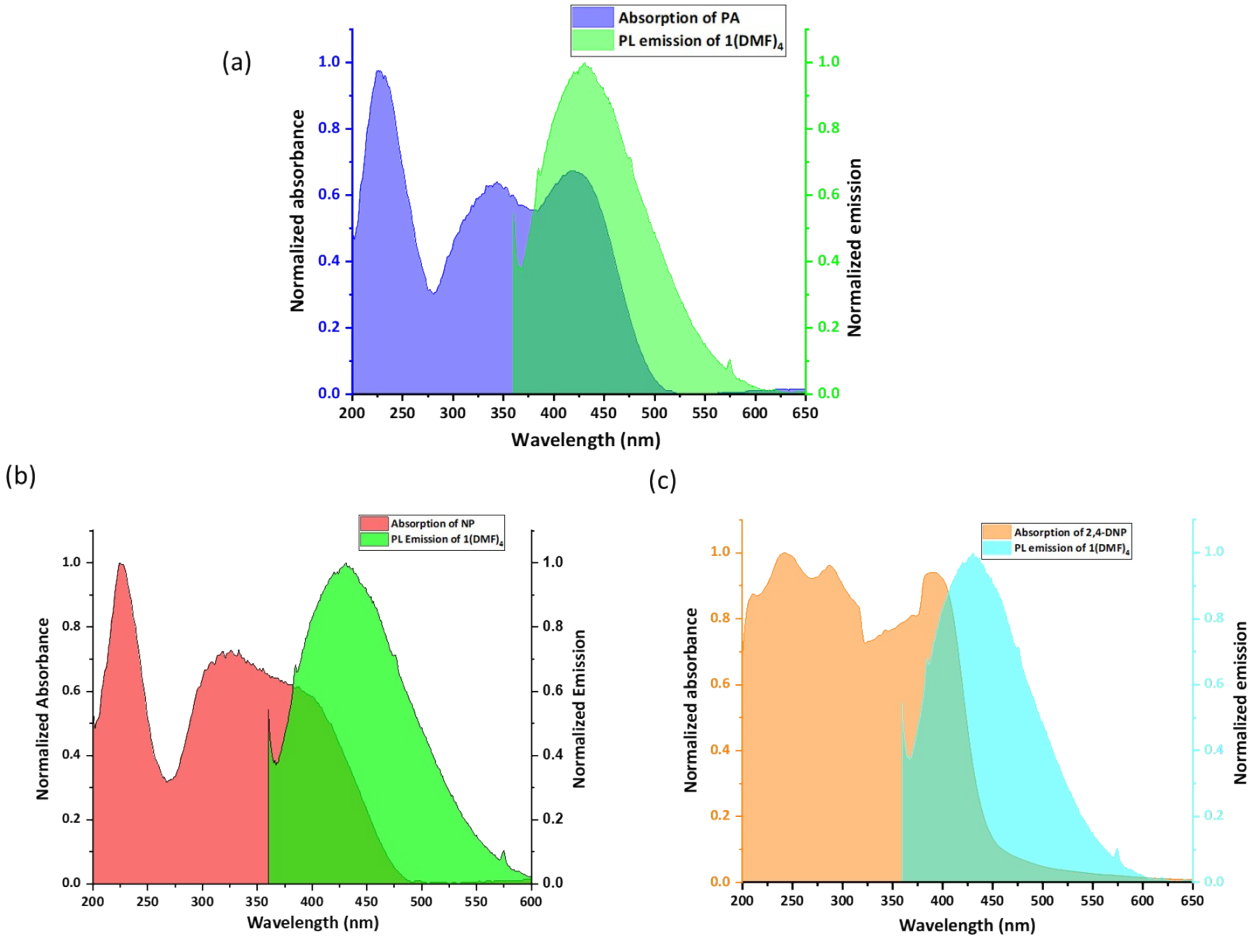

Figure S41. Overlap of emission spectra of **1(DMF)$_4$** in solid state with absorption spectrum of (a) PA (b) 4-NP (c) 2,4-DNP.

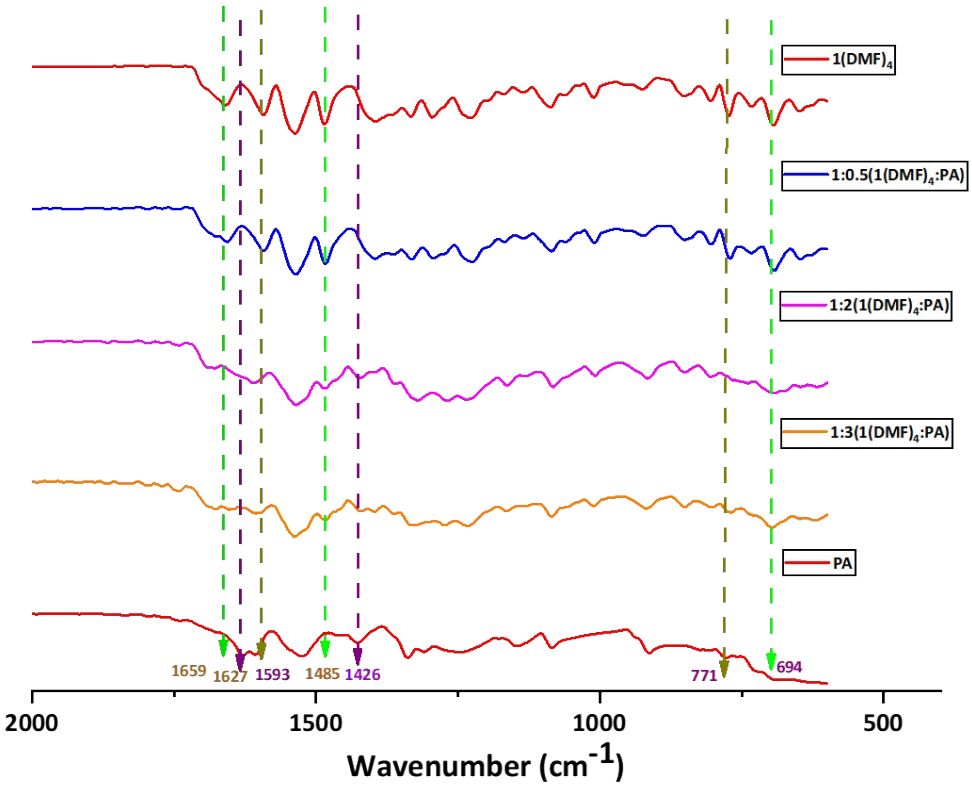

Figure S42. Comparison of IR spectra of **1(DMF)$_4$** in presence of different amount of PA: (a) **1(DMF)$_4$** only, (b) **1(DMF)$_4$**: PA = 1:0.5; (c) **1(DMF)$_4$**: PA = 1:2; (d) **1(DMF)$_4$**: PA = 1:3; (e) PA only; Note that for **1(DMF)$_4$**, asymmetric unit of **1(DMF)$_4$** is considered for calculating the ratio. (Notice the appearance of peaks corresponding to PA (some of the peaks are 1627cm^{-1}, 1426cm^{-1}) as the ratio of picric acid increases, while the original peaks of **1(DMF)$_4$** (some of the peaks are 694 cm^{-1}, 1435 cm^{-1}, 1593 cm^{-1}, 1659 cm^{-1}) are retained).

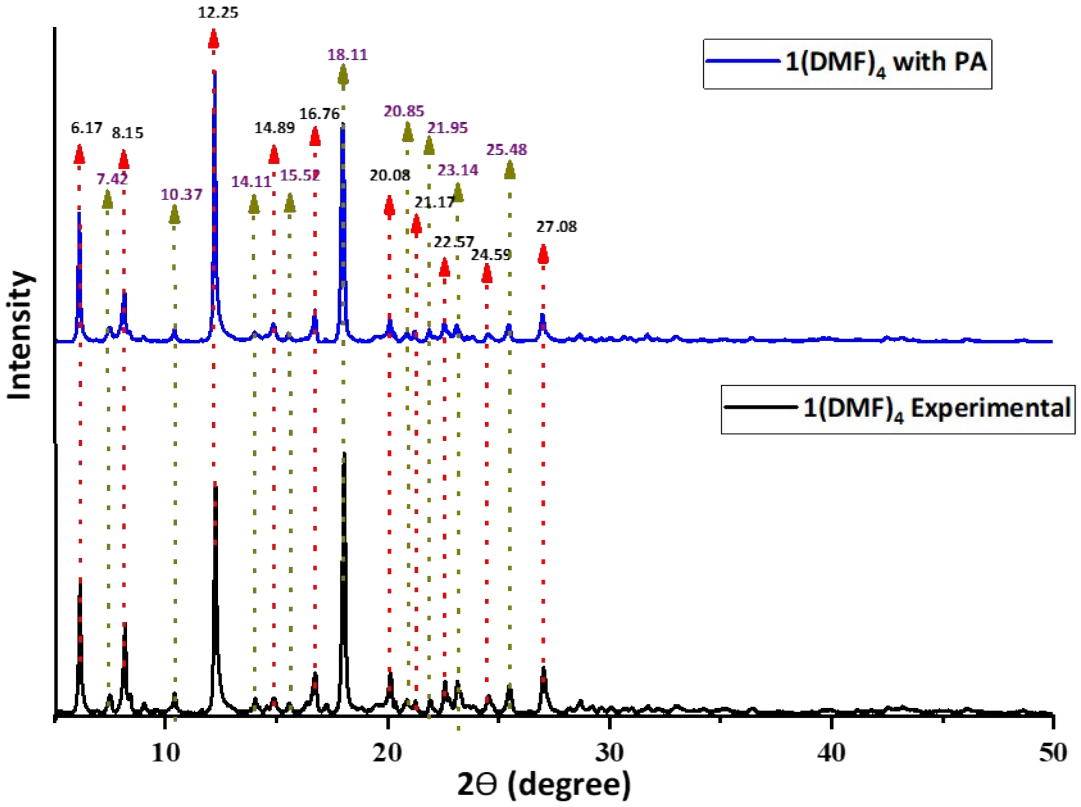

Figure S43. PXRD of **1(DMF)$_4$**: Experimental (a) **1(DMF)$_4$** and PA (b) **1(DMF)$_4$** experimental.

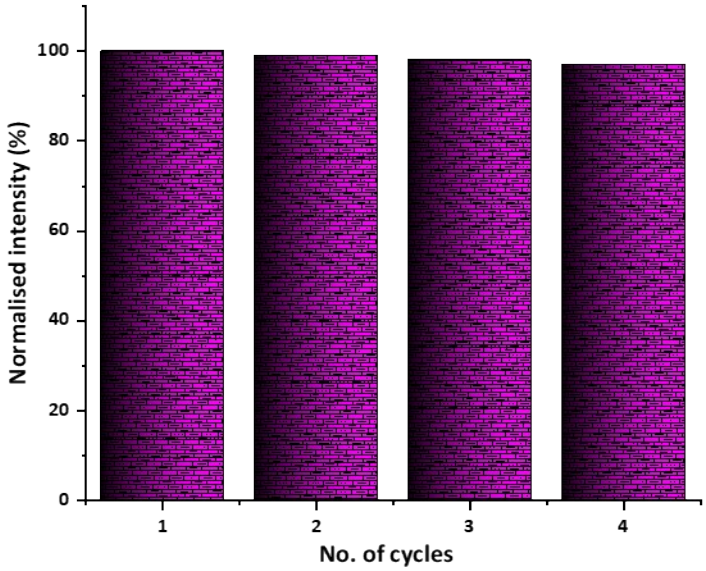

Figure S44. Fluorescence intensity after four cycles.

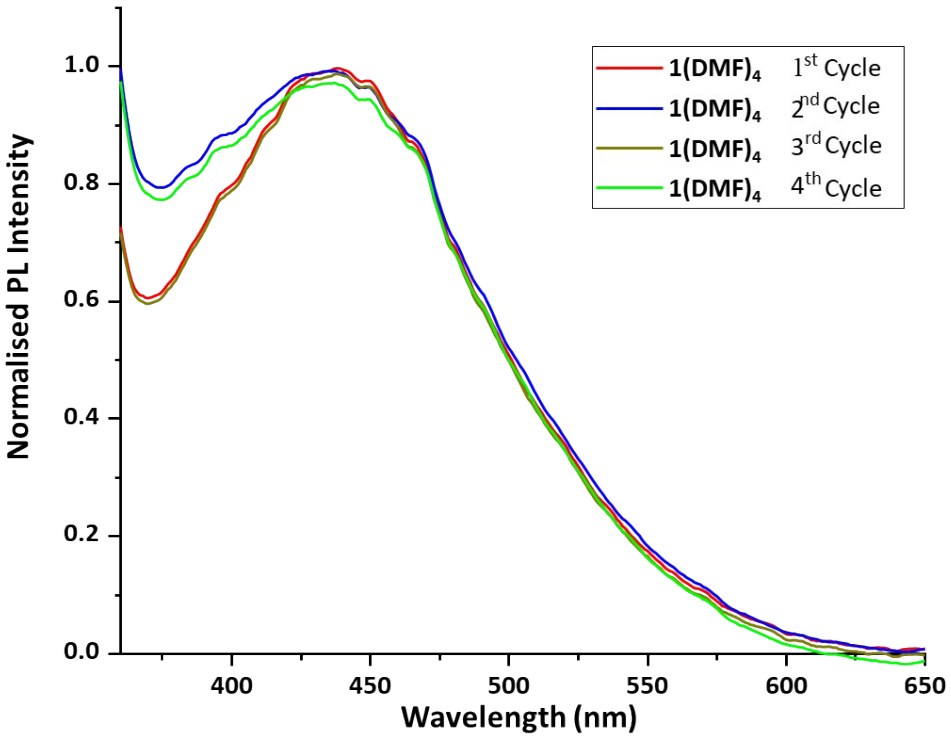

Figure S45. Emission spectra of thin film of **1(DMF)$_4$** and PA; Spectra were taken after recovering **1(DMF)$_4$** by removing PA.

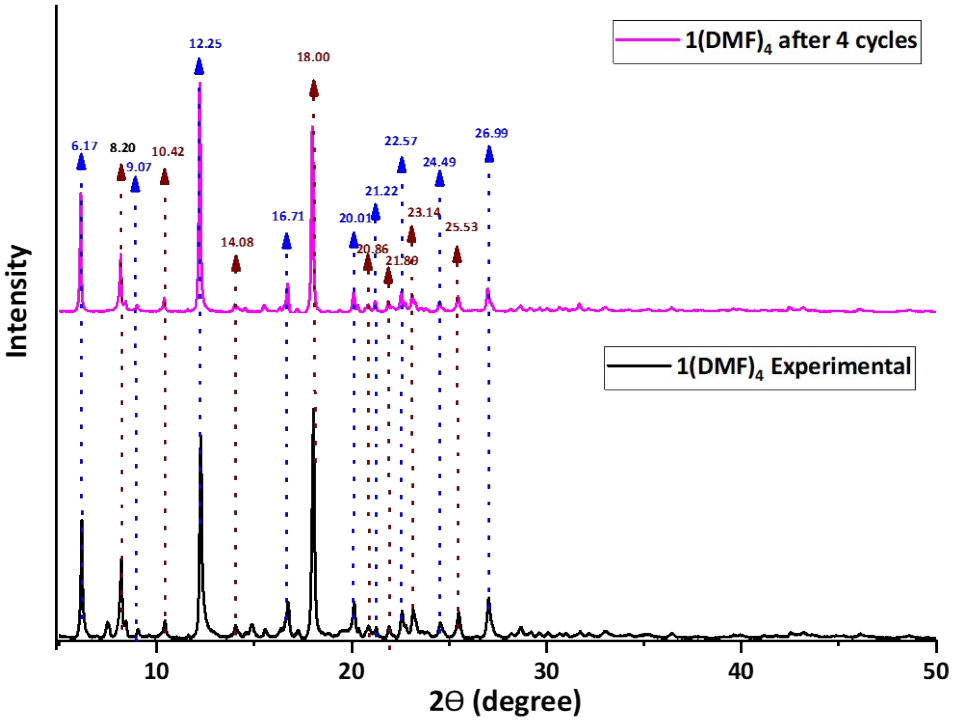

Figure S46. PXRD of **1(DMF)$_4$**: Experimental **1(DMF)$_4$** and **1(DMF)$_4$** recovered after removing PA (4th cycle).

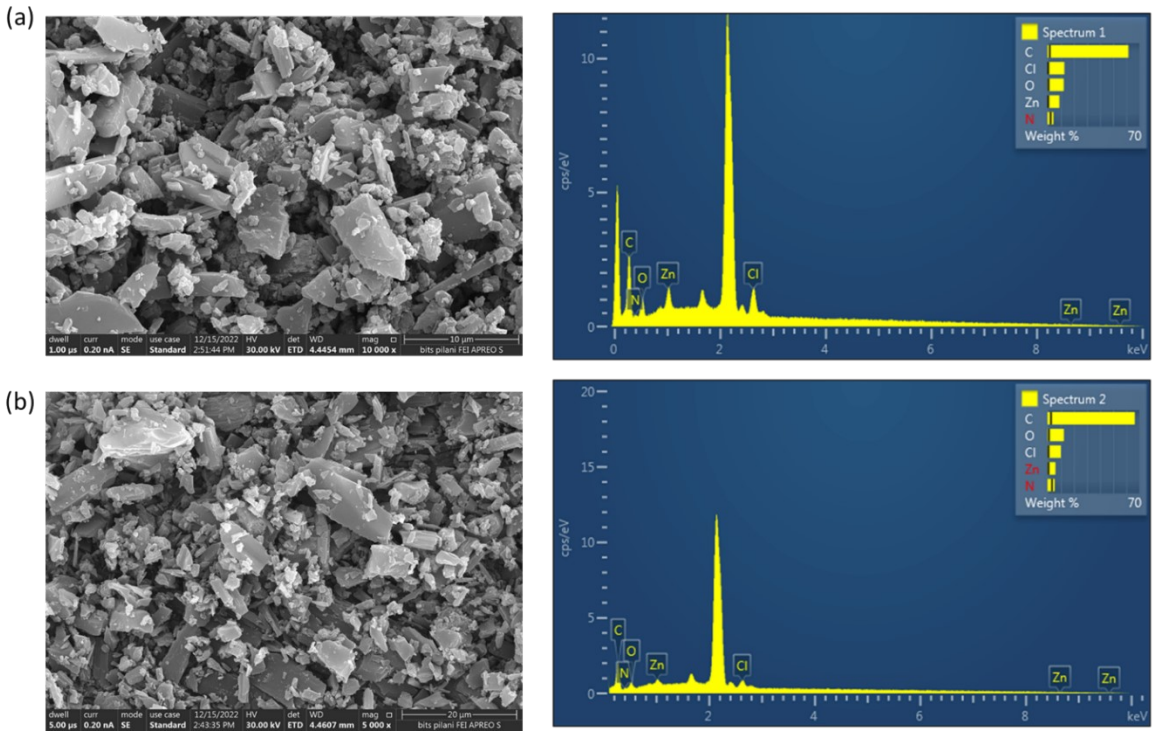

Figure S47. SEM-EDX Morphology of (a) **1(DMF)$_4$**, (b) **1(DMF)$_4$** after PA intake; Mapping of (c) **1(DMF)$_4$** [Molecular weight of **1(DMF)$_4$**:($C_{44}H_{40}N_8Cl_2O_9Zn$)=961; Molecular weight after removing DMF and hydrogen atoms =789) Observed wt.% of Zn = 8.94%; Calculated wt% Zn =8.23%] (d) 1:1 ratio of **1(DMF)$_4$** and PA (Solid sample) [Molecular weight of 1(DMF)4:PA (1:1 ratio): ($C_{44}H_{40}N_8Cl_2O_9Zn$)=961+229.1=1188.1 (Molecular weight excluding hydrogen=1145.1) Observed wt.% of Zn = 5.90%; Calculated wt% Zn =5.70%] (Asymmetric unit of **1(DMF)$_4$** is considered for calculation).

Table S1 Crystal data and structure refinement for **1(DMF)$_4$**

Empirical formula	$C_{88}H_{80}Cl_4N_{16}O_{18}Zn_2$
Formula weight	1922.22
Temperature/K	93(2)
SSSS	monoclinic
Space group	$P2_1/n$
a/Å	17.2400(3)
b/Å	11.9521(2)
c/Å	21.5421(4)
α/°	90
β/°	98.188(2)
γ/°	90
Volume/Å^3	4393.59(14)
Z	2
ρ_{calc}g/cm^3	1.453
μ/mm^{-1}	2.446
F(000)	1984.0
2Θ range for data collection/°	8.294 to 159.352
Index ranges	-21 ≤ h ≤ 21, -14 ≤ k ≤ 14, -27 ≤ l ≤ 27
Reflections collected	15886
Independent reflections	11452 [R_{int} = 0.063 (component 1 (71%) and R_{int} = 0.113 (component 2 (29%), R_{sigma} = 0.0534]*
Data/restraints/parameters	11452/0/582
Goodness-of-fit on F^2	0.987
Final R indexes [I>=2σ (I)]	R_1[a] = 0.0614, wR_2[b] = 0.1553
Final R indexes [all data]	R_1[a] = 0.0848, wR_2[b] = 0.1672
Largest diff. peak/hole / e Å^{-3}	0.89/-0.88

[a] $R_1 = \sum||F_o| - |F_c||/\sum|F_o|$. [b] $wR_2 = [\sum w(F_o^2 - F_c^2)^2/\sum w(F_o^2)^2]^{1/2}$, where $w = 1/[\sigma^2(F_o^2) + (aP)^2 + bP]$, $P = (F_o^2 + 2F_c^2)/3$.

*The crystal structure is twin modelled with component 1 (71%) and component 2 (29%).

Table S2 Bond lengths and bond angles in metal coordination sphere in **1(DMF)$_4$**

D-H…A	d(D-H)/Å	d(H-A)/Å	d(D-A)/Å	D-H-A/°
N1-H1…O8[a]	0.88	2.16	3.006(4)	160.7
N2-H2…O4[b]	0.88	2.12	2.910(4)	149.7
N3-H3…O7[b]	0.88	2.04	2.900(4)	164.5
Symmetry codes: [a]+x,+y,+z;[b]+x,1+y,+z.				

Table S3 Distances and angles in hydrogen bond interactions in **1(DMF)$_4$**

Bond Lengths			Bond Angles			
Atom1	Atom2	Length (Å)	Atom1	Atom2	Atom3	Angle (°)
Zn1	O4	2.016(2)	O4	Zn1	O5	57.9(1)
Zn1	O5	2.446(3)	O4	Zn1	O6	96.2(1)
Zn1	O6	1.980(3)	O4	Zn1	N4	138.4(1)
Zn1	N4	2.020(3)	O4	Zn1	N5	102.8(1)
Zn1	N5	2.053(3)	O5	Zn1	O6	154.0(1)
			O5	Zn1	N4	91.4(1)
			O5	Zn1	N5	90.9(1)
			O6	Zn1	N4	109.2(1)
			O6	Zn1	N5	98.5(1)
			N4	Zn1	N5	105.2(1)

S.No.	Compound	Concentration of 1(DMF)$_4$	Concentration of PA	Lifetime (ns)
1.	**1(DMF)$_4$**	10^{-5}M	-	0.36 ns
2.	Solution 1	10^{-5}M	5×10^{-7} M	0.35 ns
3.	Solution 2	10^{-5}M	1.5×10^{-6} M	0.34 ns
4.	Solution 3	10^{-5}M	3×10^{-6} M	0.34 ns
5.	Solution 4	10^{-5}M	4.5×10^{-6} M	0.33 ns
6.	Solution 5	10^{-5}M	6.5×10^{-6} M	0.32 ns

Table S4 Lifetime data of **1(DMF)$_4$**. (Lifetime plots are shown in fig. S20)

Table S5 Photophysical data of **1(DMF)$_4$** in DMSO and solid state (Absorption and emission plots are shown in fig. S10 and S11)

S.No.	Photophysical Data	**1(DMF)$_4$** in DMSO	**1(DMF)$_4$** in Solid State
1.	UV Maxima (λ_{max}, ε)	278 nm, 38959 M^{-1} cm^{-1}	245 nm and 290 nm
2.	PL Maxima (λ_{em}, Stoke shift)	409 nm, 169491.53 cm^{-1} (Slit Width = 4 nm)	430 nm, 125000 cm^{-1} (Slit Width = 2.5 nm)
3.	Quantum Yield (ϕ)	0.4 %*	6.03 %*
* Absolute quantum yield			

Table S6 Comparison of **1(DMF)$_4$** with literature reports

Type of Probes	Reported Probes	Detection Limit / Medium	K_{sv} Value
Metallocycles/Metal Organic Cages	**This work**	6.89×10^{-11} M of picrate ion in liquid state (DMSO) and 0.49 ng/cm^2 of picric acid in solid state.	5.174×10^4 M
	Pd-Macrocycle (1&2)[1]	287 nm & 71 nm in EtOH	6.73×10^4 M and 2.61×10^5 M
	Re(I)-metallacycles (3b & 4)[2]	Medium= 60% aqueous THF solution	2.6×10^4 M and 4.38×10^4 M
	Zn (II)- metallacycle[3]	7.62×10^{-8} M in 50% H_2O: EtOH	3.44×10^4 M
	Pt (II) - metallacycle[4]	3.01×10^{-7} M in CH_2Cl_2	1.3×10^5 M^{-1}
	3d – 4f metal–organic cages (1&2)[5]	79 ppb and 60 ppb in DMSO (LOD = $C_s \times D_a$) C_s is concentration of sensors and D_a is equivalent of PA	7.79×10^4 M^{-1} and 1.33×10^5 M^{-1}
	Pt^{II}_2-organometallic (2&3)[6]	Medium = DMF – methanol solution	2.0×10^4 M^{-1} and 5.0×10^4 M^{-1}
Metal Organic Framework	**Ni-OBA-Bpy-18 MOF/glassy carbon electrode[7]**	66.43 ppb in vapour phase and water 0.6 ppm	3.45×10^5 M^{-1}
	$\{[Eu_2(MFDA)_2(HCOO)_2(H_2O)_6]\cdot H_2O\}^8_n$	4.5×10^{-7} M in DMF	-
	CJLU-1[9]	0.362 μM in ethanol	2.60×10^5 M^{-1}
	$\{Zn_2(tpt)_2(tad)_2\cdot H_2O\}$[10]	2.56×10^{-6} M in water	7.8×10^4 M^{-1}

References.

1. S. Kumar, R. Kishan, P. Kumar, S. Pachisia and R. Gupta, Inorganic Chemistry, 2018, **57**, 1693-1697.
2. M. Nurnabi, S. Gurusamy, J.-Y. Wu, C.-C. Lee, M. Sathiyendiran, S.-M. Huang, C.-H. Chang, I. Chao, G.-H. Lee, S.-M. Peng, V. Sathish, P. Thanasekaran and K.-L. Lu, Dalton Transactions, 2023, **52**, 1939-1949.
3. P. Chand and A. Kumar, New Journal of Chemistry, 2024, **48**, 11530-11541.
4. Y. Hou, S. Li, Z. Zhang, L. Chen and M. Zhang, Polymer Chemistry, 2020, **11**, 254-258.
5. Q. Tang, Y. Sun, H.-Y. Li, J.-Q. Wu, Y.-N. Liang and Z. Zhang, Applied Organometallic Chemistry, 2019, **33**, 4814.
6. S. Shanmugaraju, S. A. Joshi and P. S. Mukherjee, Inorganic Chemistry, 2011, **50**, 11736-11745.
7. S. Chongdar, U. Mondal, T. Chakraborty, P. Banerjee and A. Bhaumik, ACS Applied Materials & Interfaces, 2023, **15**, 14575-14586.
8. X.-H. Zhou, L. Li, H.-H. Li, A. Li, T. Yang and W. Huang, Dalton Transactions, 2013, **42**, 12403-12409.
9. H. Xu, F. Zhong, F. Chen, T.-X. Luan, P. Li, S. Xu and J. Gao, Journal of Materials Chemistry C, 2022, **10**, 7469-7475.
10. X. Zhuang, X. Zhang, N. Zhang, Y. Wang, L. Zhao and Q. Yang, Crystal Growth & Design, 2019, **19**, 5729-5736.